TAMPEREEN TEKNILLINEN YLIOPISTO
TAMPERE UNIVERSITY OF TECHNOLOGY

MATTI KESTI

DEVELOPMENT OF 3D BIOPRINTING INKS BASED ON TANDEM CROSSLINKED HYDROGELS

Master's thesis

Examiner : Minna Kellomäki
Inspected and approved in the
faculty of materials science
18th of September 2013, Zurich

TIIVISTELMÄ

TAMPEREEN TEKNILLINEN YLIOPISTO
Materiaalitekniikan koulutusohjelma
KESTI, MATTI: Development of 3D bioprinting ink based on tandem crosslinked hydrogels
Diplomityö, 50 sivua, 2 liitesivua
Syyskuu 2013
Pääaine: Biomateriaalitekniikka
Tarkastaja: Professori Minna Kellomäki
Avainsanat: Pikavalmistus, 3D tulostus, nivelrusto korjaus, UV-ristisilloittuminen, lämpöherkkä ristisilloittuminen, HA-PNIPAM

Tulevaisuudessa lääketiede suuntautuu yhä vahvemmin räätälöityjen hoitomenetelmien sekä potilaskohtaisten implanttien käyttöön. Potilaskohtaisen implantin tulee olla suunniteltu juuri kyseisen potilaan tarvetta varten esimerkiksi muotonsa osalta ja siinä käytettyjen solujen tulee olla peräisin potilaasta itsestään. Näin ollen implantti jäljittelee luonnollista kudosta ja on täysin bioyhteensopiva ympäröivän kudoksen kanssa. Pikavalmistuksen avulla potilaskohtaisten implanttien valmistus on jo mahdollista ja yhtenä valmistusmenetelmänä käytetään biotulostusta.

Tämän diplomityön tarkoituksena oli tutkia erilaisten materiaaliyhdistelmien käyttöä biomusteena nivelruston tulostuksessa. Työssä suunniteltiin ja tutkittiin kolmea rustolle suunniteltua kaksois-ristisilloittuvaa hydrogeeli biomustetta. Tulostettavuuden ja resoluution osoittamiseksi näillä materiaaleilla tulostettiin erilaisia muotoja ja komposiittirakennelmia, joiden muotoa ja kokoa analysoitiin. Tulostuksessa käytetyt materiaalit olivat hyaluronaani, kondroitiinisulfaatti ja dextran, jotka olivat käyneet läpi metakrylointireaktion. Nämä materiaalit sekoitettiin hyaluronaanin kanssa, joka oli polymeroitu poly(N-isopropyyliakryyliamini) (PNIPAM) sivuryhmällä.

Käytetyt kaksiosaiset yhdistelmämateriaalit ovat ainutlaatuisia käyttäen HA-PNIPAM-materiaalia 3D-biotulostuksessa sekä yhdistäen kaksois-ristisilloituksessa UV- ja lämpöherkkiä polymeerejä. Yhdistäen nämä materiaalit saimme aikaan kolme biomustetta, jotka jäljittelevät nivelruston kerroksellista rakennetta. Nämä yhdistelmämateriaalit pysyivät muodossaan tulostuksen jälkeen ja niiden moduulia pystyttiin kasvattamaan UV-käsittelyllä. Valmiiden implanttien moduulit ovat vielä riittämättömiä polvirustoimplanteiksi, mutta niiden tulostettavuus ja saavutettu resoluutio ovat tarvittavalla tasolla. Tulevaisuudessa lämpöherkkän ristisilloittumisen kontrolloitavuutta tulisi kehittää ja luoduille biomusteille tulisi suorittaa solukokeita bioyhteensopivuuden varmistamiseksi.

ABSTRACT

TAMPERE UNIVERSITY OF TECHNOLOGY
Master's Degree Programme in Materials Science
KESTI, MATTI: Development of 3D bioprinting ink based on tandem crosslinked hydrogels
Master of Science Thesis, 50 pages, 2 Appendix pages
September 2013
Major: Materials Science
Examiner: Professor Minna Kellomäki
Keywords: Rapid prototyping, 3D bioprinting, cartilage, UV crosslinking, thermo sensitive crosslinking, HA-PNIPAM

In the future the field of medicine will be directed towards tailored treatments and personalized medicine. In personalized medicine the implant is designed for the patient's needs in terms of the shape of the implant and the cells encapsulated into the implant, which are harvested from the patient itself. By these means, the produced implant is mimicking the designated tissue and the cells are fully biocompatible with the surrounding tissue. By utilizing rapid prototyping in biomaterial scaffold or tissue graft production, the patient optimized implants could be produced. One promising rapid prototyping technique is bioprinting.

The aim of this thesis was to investigate different material combinations to be used as bioinks for cartilage production. In this thesis, three cartilage specific tandem crosslinked hydrogel bioinks were created and analyzed. Furthermore, different constructs and printed composite structures were created to prove the printability and resolution of these bioinks. Materials used in this study were hyaluronic acid, chondroitin sulfate and dextran which were grafted with methacrylate groups. These materials were mixed with hyaluronic acid grafted with poly(N-isopropylacrylamine) (HA-PNIPAM).

The two-component hydrogels used were novel in regards to utilize HA-PNIPAM in 3D bioprinting and in using tandem crosslinking combining thermo and photosensitive crosslinking in the printing. By combining the two crosslinking methods we were able to create three different bioinks mimicking the cartilage layered structures. Tandem crosslinked bioinks kept the resolution of the printing process and they had an increased modulus after UV curing. The implants produced had insufficient mechanical properties compared to native cartilage, however, the printability and the resolutions were on sufficient levels. Further development to control the temperature gelation is required and the viability assays for the bioinks should be investigated.

PREFACE

This Master of Science thesis was made at ETH Zurich in Switzerland. The whole thesis process lasted for seven months between February 2013 and August 2013. I started writing the thesis after working six months in AO research institute Davos in Switzerland as a trainee. From this internship I got the background knowledge for the hyaluronan materials and the cooperation in using HA-PNIPAM in my thesis was started. This supporting network from both ETH Zurich and AO Institute Davos helped me during the thesis project. During the master's project I had to learn lots of new about cell studies and at the end it was both challenging and rewarding.

First of all, I would like to thank Professor Marcy Zenobi-Wong for giving me the opportunity to do my master's thesis in ETH Zurich and for guiding me through the project. I would also like to thank Professor David Egling for providing HA-PNIPAM materials and for all his advices during the project. I would also like to thank Professor Minna Kellomäki for examining the final thesis and for taking care of the documents for the TUT on my behalf. I would like to thank especially Mischa Müller for mentoring me during the thesis and examining this thesis. Furthermore, I would like to thank the cartilage group in ETH for the great support I got and the enormous help I received.

Furthermore, I wish to thank my amazing friends and family who supported me during my studies and in the thesis project.

Zurich, 20th August 2013

Matti Kesti

LIST OF SYMBOLS AND ABBREVIATIONS

G’	Starage modulus
G’’	Loss modulus
AC	Articular cartilage
ACT	Autologous chondrocyte transplantation
bCh	Bovine chondrocyte
Bioink	Biological ink used in bioprinting
COMP	Cartilage oligomeric matrix protein
CSMA	Chondroitin sulfate grafted with methacrylate
CT	Computed tomography
DEXMA	Dextran grafted with methacrylate
DIW	Direct ink writing
DMD	Digital micro-mirror device™
DMEM	Dulbecco’s modified eagle medium
EASP	Extrusion/aspiration patterning
ECM	Extra cellular matrix
GAG	Glycosaminoglycan
^{1}H-NMR	Nuclear magnetic resonance spectroscopy for proton
HA-PNIPAM	Hyaluronic acid poly(N-isopropylacrylamine)
HAMA	Hyaluronic acid grafted with metacrylate
HA-TBA	Hyaluronic acid tetrabutylammonium salt
HM_W	High molecular weight
LAP	lithiumphenyl-2,4,6-trimethylbenzoylphosphinate photoinitiator
LCST	Lower critical solution temperature
LDM & M-LDM	Low-temperature deposition modeling & multiple nozzle low-temperature deposition modeling
LM_W	Low molecular weight
MRI	Magnetic resonance imaging
MTT	(3-(4,5-dimethylthiazol-2-yl)-2,5-diphenyltetrazolium bromide
OA	Osteoarthritis
PAM	Pressure-assisted microsyringe
PBS	Phosphate buffer saline
RP	Rapid prototyping
SGC	Solid ground curing
SLA & u-SLA	Stereolitography & micro stereolitography
TGA	Thermal gravimetric analysis
UV	Ultraviolet light
2PP	Two photon-polymerization

CONTENTS

1. INTRODUCTION

Three dimensional tissue printing is a new and revolutionary technique towards personalized medicine. With 3D bioprinting, a patient specific and uniquely designed tissue graft could be manufactured by means of magnetic resonance imaging (MRI) data. These designed tissue grafts would not only fit to the patient's defect but also mimic the native articular cartilage layered structure. Articular cartilage (AC), which composes of three different zones: superficial, intermediate and the deep, can be found in each joint in the body. These zones vary significantly throughout the structure in terms of modulus, cell concentration and water content (Blitterswijk et al. 2008). AC cells, chondrocytes, proliferate in an avascularized tissue under hypoxia conditions which limits their ability to regenerate damaged cartilage. Due to this fact, an injury or development of osteoarthritis in the articular cartilage represents a challenging clinical problem. Sports related injuries in the knee joint including meniscus tear and articular cartilage wearing are common within the younger patients. These patients are at higher risk in wearing of the repaired knee or of developing osteoarthritis. Osteoarthritis (OA) affecting articular cartilage is a major challenge especially in aging population due to decreased chondrocyte activity in aging and increased potential for development of an OA condition. The chance of developing the disease increases with age and about 6% of adults aged 30 have frequent knee pain and radiographic evidence of OA. Symptomatic knee OA affects 12% of people over 65 years of age (Warrell et al. 2010; Peach et al. 2005; Vincent and Watt, 2010). OA is not a localized condition, but rather affecting multiple joints simultaneously, which undermines extensive need for the cartilage regenerative medicine. In 2007 only in US more than 400 000 cartilage related procedures were performed with an estimated market value of approximately 55 million dollars. Further estimations for the potential market for advanced cartilage therapies could reach to 500 000 procedures with a value of 1.5 billion dollars (MeNickle et al., 2008).

Cartilage tissue engineering research has expanded at a fast rate during the last decade. As in the field of tissue engineering, the investigation of hydrogels has become prominent in cartilage research (Peroglio et al., 2012, Fedorovich et al., 2007). Hydrogels provide interesting properties for cartilage tissue engineering as they bind significant amounts of water in their structure like in the native articular cartilage surface. Furthermore, these hydrogels properties can be tailored to mimic the natural extra cellular matrix (ECM) of the implantation site to provide enhanced biocompatibility with the cells. The hydrogel tailoring can be done by choosing glycoseaminoglycans (GAG) present in the AC ECM such as hyaluronic acid and chondroitin sulfate (Temenoff and Mikos,

2000). Furthermore, the hydrogel properties are tailored by affecting concentrations, grafting densities, crosslinking densities and crosslinking methods. Several different crosslinking methods including pH, temperature, UV-light and radical crosslinking have been investigated for the cell encapsulation and drug delivery applications (Chaterji et al., 2007). Depending on the hydrogel materials and structures, the properties of the hydrogels can vary significantly. Due to the complex structures of the native tissues, such as the layered structure of the articular cartilage, defined structured hydrogels are needed. To produce complex and precise hydrogel structures, rapid prototyping (RP) techniques have been utilized. Hydrogels have been developed extensively for different RP techniques for tissue engineering purposes. Various RP techniques such as 3D bioprinting utilize hydrogels for cell encapsulation and drug delivery structures. (Billiet et al., 2012, Peltola et al., 2008). Rapid prototyping techniques including laser based, nozzle based and printer based systems are intensively studied and developed to produce highly sophisticated hydrogel structures for tissue engineering. However, as stated in the review article by Fedorovich et al. the future direction of organ printing with hydrogels include the development of better hydrogels, with emphasis on mechanical properties and degradation rates (Fedorovich et al., 2007). Mainly due to insufficient mechanical properties hydrogels have not been utilized in load bearing applications.

Bioprinting, a subgroup of rapid prototyping, requires the development of biological inks (bioink). An optimal bioink is a balance between four requirements: handling, printability, mechanical properties and biocompatibility. Regardless of the tissue type these requirements stay and they are all equally important as illustrated in Figure 1.1. The handling, printing and biocompatibility of the ink should be always kept the highest possible regardless of the desired tissue. The mechanical properties of the ink refers to printability, however, the mechanical properties of the hydrogel construct can be mainly influenced by changing the ink composition rather than structure or printing parameters. The bioink composition affects also to the crosslinking behavior and possibly even crosslinking method. Temperature crosslinking is an effective crosslinking method in printing techniques; due to small dispensing volumes the temperature shift is almost immediate. However, the temperature crosslinking does not provide enough stability for in vivo implantation since it is not covalently cross-linked, which also makes the crosslinking reversible. Inversely, the photosensitive crosslinking is providing stabile structures with significantly higher modulus but the reaction between the photoinitiator and the acrylic based groups is slower. This delayed crosslinking allows flow of the structure and the resolution of the printing is lost.

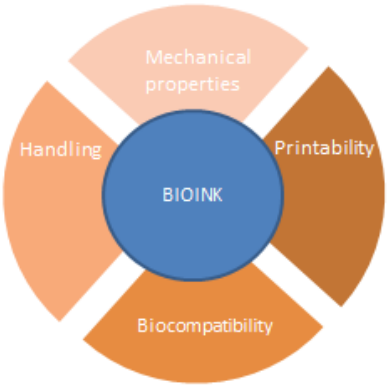

Figure 1.1. *Four requirements of a bioink are illustrated.*

Aim of this thesis was to investigate different material combinations to be used as bioinks for cartilage production. The mechanical properties of the crosslinked gels were analyzed and compared in different biopolymer concentrations. Based on these results as well as biocompatibility assays, the promising gel mixtures were chosen and used for bioprinting. Furthermore, different constructs and printed composite structures were created and analyzed. Materials used in this study were hyaluronic acid, chondroitin sulfate and dextran which were derivatized with methacrylates, and each of the materials was mixed with hyaluronic acid grafted with poly(N-isopropylacrylamine). These two component hydrogels were novel in utilizing HA-PNIPAM in 3D bioprinting and in combining tandem crosslinking with thermo and photosensitive crosslinking. By combining the thermo and photosensitive crosslinking we were able to create three different bioinks mimicking the cartilage layered structures. Tandem crosslinked bioinks held the resolution of the printing and had increased modulus after UV curing.

2. RESEARCH OVERVIEW

The thesis consists of three parts: 1) preparation of hydrogels and optimization of mechanical properties, 2) Cell viability and differentiation studies for the encapsulated chondrocytes, and 3) Bioprinting of the promising bioinks in articular cartilage layered mimicking 3D structures.

2.1. Goal of the study

The main goal of this thesis was to investigate and develop functional bioinks for cartilage bioprinting applications. These bioinks were developed especially for cartilage tissue engineering trying to mimic the extra cellular matrix produced by the chondrocytes in native articular cartilage.

2.2. Research summary

This goal was pursued starting from combining thermoreversibel HA-PNIPAM with photosensitive polymers such as hyaluronic acid, dextran and chondroitin sulfate, all methacrylated. In the first phase the extensive rheology testing was carried out to investigate the crosslinking kinetics of each individual polymer and their mixtures. The polymer blends proven to be tandem crosslinkable were further studied for their printability. Furthermore, in the second phase these material blends and individual biopolymers were mixed with bovine chondrocytes and gelled for cell encapsulation and viability studies. In the last phase the chosen bioinks were printed individually and together to produce different structures. Structure mimicking the three layers of cartilage was successfully printed using the bioink materials. Future studies will consider the in vitro cell studies for the 3D cartilage graft construct.

3. CARTILAGE

Cartilage, formed by chondrocytes, can be found in several places in the body. These different places require optimized cartilage composition and this is why three different cartilage types can be identified 1) hyaline cartilage from joints, rib cartilage, nose, trachea and larynx; 2) elastic cartilage from ear, epiglottis and larynx and 3) fibrous cartilage from intervertebral discs (Blitterswijk et al. 2008). Apart from this, hyaline cartilage is also present in bone maturation through the process called endochondral ossification. Figure 3.1 illustrates the structure of the hyaline articular cartilage in the adult knee joint. The magnification of the articular cartilage reveals the layered structure which is in average 2.4 mm thick in the loaded areas such as joints. The biggest magnification illustrates the most important components present in AC. The ratio of each component is changing throughout the layered structures so that the layers have different properties. Cartilage consists only of 2% chondrocytes, 20-35% of other components and 65-80% of water. The more specific ratio of polymeric component is about 60% collagen mainly type II and X, 30% proteoglycans (Becerra et al. 2010; Blitterswijk et al. 2008). Collagen II is the main type of collagen (90%) encountered in adult healthy cartilage and it is responsible for the tensile strength of the cartilaginous surface (Figure 3.1). Cartilage integrates in its structure a great amount of proteoglycans that consist of a core protein with many glycosaminoglycans attached to it in a brush-like fashion. This specific structure slows down the escape of water under mechanical loading and is responsible for the great compressive strength of the cartilage (Becerra et al. 2010). Articular cartilage compressive strength has been studied by (Gigante et al., 2001) and the compressive modulus of 0.79 MPa, shear modulus of 0.69 MPa and the tensile modulus of 0.3 – 10 MPa were identified. Furthermore the bovine articular cartilage viscoelastic properties has been investigated by (Fulcher et al., 2009). This study revealed the high storage modulus (G') values 50.1 MPa ± 12.5 MPa and loss modulus (G'') values 4.8 MPa ± 1.0 MPa for the articular cartilage.

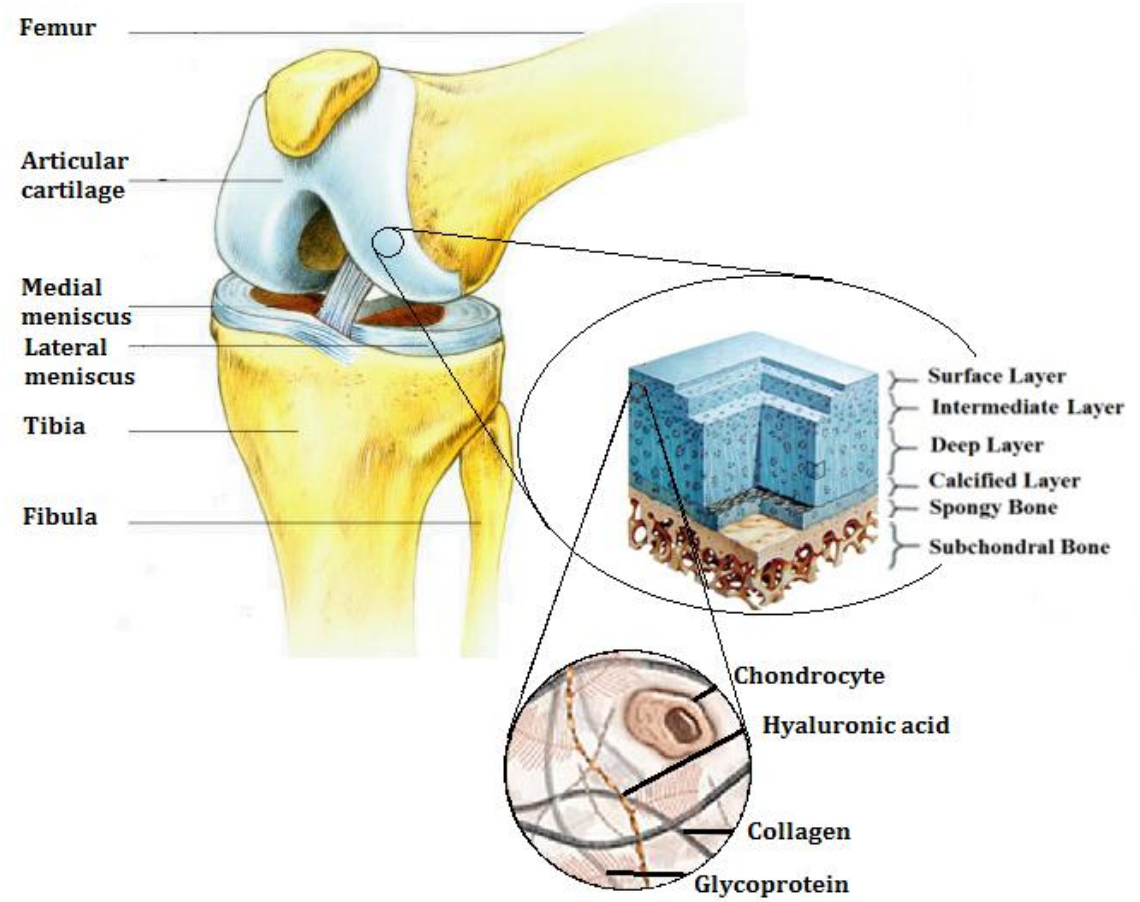

Figure 3.1. *Schematic picture of hyaline articular cartilage and its composition. Magnification from the knee joint shows the layered structure of articular cartilage and further the most important components of the cartilage ECM Modified from (Duracon; Landinez-Parra, 2012).*

Aggrecan, biglycan, decorin, fibromodulin, the matrilins, and cartilage oligomeric matrix protein (COMP) are the major proteoglycans found in cartilage (Blitterswijk et al. 2008). Aggrecan for example consists of chondroitin sulfate and keratin sulfate which brushes out from the core proteoglycan to give aggrecan its well known shape (Fosang et al., 1992). These aggrecan molecules are responsible of lubrication in the surface (Blitterswijk et al. 2008).

Chondrocytes are the only type of cells found in articular cartilage, and are not in direct contact with the load-bearing matrix but are protected by a microenvironment called chondron (Ashammakhi et al. 2007; Goessler et al. 2006). Chondrocytes are nutritioned by the blood circulation in subchondral bone and bone marrow. The synovial fluid between the cartilage surfaces in the joint is also supporting chondrocyte nutrient and waste management (Blitterswijk et al. 2008). Self-repair possibilities of cartilage are extremely limited after an injury due to the lack of blood supply, the low turnover rate of chondrocytes and sparsely distribution of chondrocytes. For this reason, several strategies for enhanced cartilage reparation has been developed. Table 3.1 summarizes most of the techniques used in clinics for cartilage reparation. The most advanced one in use being autologous chondrocyte transplantation (ACT) in which the surgeon performs a biopsy from the intact cartilage. The biopsy sample is treated by enzymes for the chon-

drocyte harvest and further in vitro expansion. After the desired chondrocyte population is expanded the cells are re-implantation (Ashammakhi et al. 2007; Blitterswijk et al. 2008).

Table 3.1: Current therapeutic techniques for treatment of articular cartilage damage (Ashammakhi et al. 2007).

Methods	Techniques	Disadvantage
I-Lavage and arthroscopy		
Lavage	Irrigation of a joint with solutions of NaCl, Ringer or Ringer and lactate.	Only short term pain relief. No solid evidences of any biological or repair activity being investigated.
II-Debridement		
Shaving and debridement of cartilage	Mechanical removal of diseased chondral tissue.	Instability of the joint.
Thermal chondroplasty (laser and radiofrequency)	Alternative debridement by heat or radiofrequency energy.	High rate of re-injury and tissue necrosis by thermal damage.
III-Marrow Stimulation Techniques		
Abrasion chondroplasty Multiple drilling (Pridie drilling) Microfracture	All these techniques involve surgical access to the subchondral bone until bleeding occurs inducing spontaneous repair responses.	Repair tissue becomes fibrocartilaginous (less durability and strength). Restriction of mobility.
IV-Transplantation		
Autologous grafting (periosteal/perichondrial/ osteochondral plug transfer)	Replace lost cartilage with tissue grafts from own patient.	Poor fixation of graft to damage area. Inflammatory and joint mobility restriction. Donor site morbidity and availability. Immunological reaction and disease transmission.
Allogeneic grafting	Replace lost cartilage with tissue grafts from different individuals.	Limited supply of graft. Handling and storage of frozen tissue.
V-Cell-based therapies		
Autologous Chondrocyte Transplantation (ACT)	Removal of patient own cells by biopsy. in vitro cell culture and implantation into defect under a periosteal patch.	Expensive treatment. Two surgical procedures needed. Potential damage to surrounding cartilage. Restricted activity to allow cell integration. Long term degeneration. Only animal models so far.

Another approach to heal cartilage defects is tissue engineering. This approach utilizes biomaterials as ECM mimicking supports for the re-implanted cells. Used biomaterials are typically biocompatible and biodegradable and they are processed to scaffolds in which autologous cells are incorporated. Many different materials have been proposed as scaffolds such as non-woven meshes and foams of alpha-hydroxypolyesters (Schulze-Tanzil, 2009), polyglactin (Müller et al. 2008), hyaluronan alkyl esters, photocross-linked hydrogels (Leach et al. 2002) and sponges based on different types of collagen

and glycosaminoglycans (Chaterji et al. 2007). Scaffolds filled with cells embedded in a fibrin or alginate gel have also been proposed (Mastbergen et al. 2002; Ceresa, 2012).

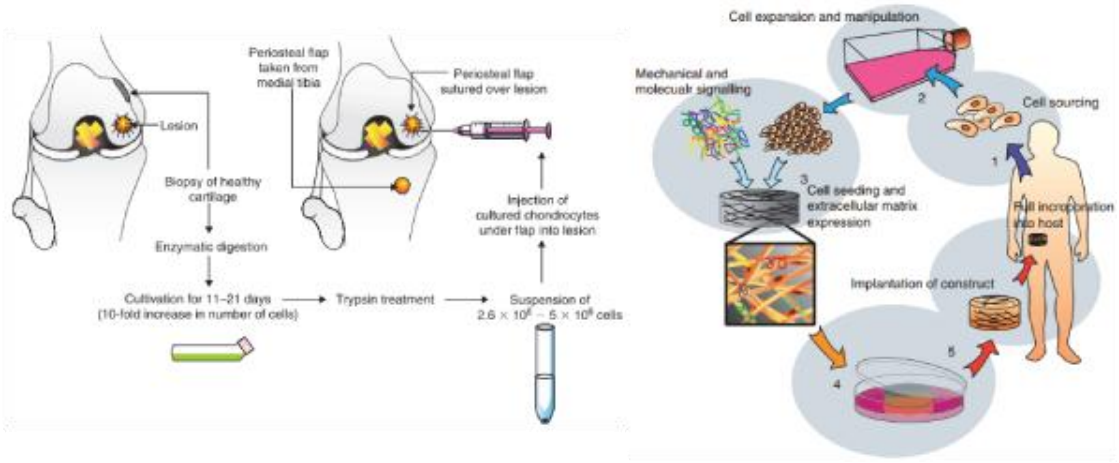

Figure 3.2. *Autologous chondrocyte transplantation and tissue engineering transplantation are illustrated. Tthe tissue engineering approach can be done without mechanical or molecular signals such as growt factors (Blitterwijk et al. 2008).*

As shown in Figure 3.2, the development of efficent in vitro culture techniques for chondrocyte expansion is needed. These in vitro expansions are typically done in 2D systems in which the chondrocytes tend to lose their phenotype and dedifferentiate towards fibroblast-like cells (Ashammakhi et al. 2007). These less specialized cells produce an unorganized and mechanically inferior matrix not suitable for cartilage regeneration treatments. Furthermore, the pericellular matrix (chondron) surrounding the chondrocytes in their native environment is absent and the ECM proteins produced are collagen type I and III instead of collagen type II. Collagen type I is normally absent in native cartilage tissue. (Becerra et al. 2010) The production of large aggregating GAGs such as aggrecan is decreased and the lower molecular weight molecules like versican are produced (Ashammakhi et al. 2007). In monolayer cultures of chondrocytes, it has been reported that an increased cell density as well as early passage number (P<4) were parameters that help to maintain the phenotypic traits to some extent (Schulze-Tanzil, 2009). Also, dedifferentiated chondrocytes can regain their phenotype when cultured in 3D after expansion (Foldager et al. 2011). For these reason, it is important for the better tissue engineering approaches to develop hydrogel based 3D cartilage repair techniques.

4. HYDROGELS IN RAPID PROTOTYPING

Hydrogel materials provide interesting properties as scaffold materials for tissue engineering. Hydrogels have been studied for drug delivery applications and soft tissue implants. Hydrogels can be tailored to mimic natural extra cellular matrix in implantation site to provide better biocompatibility. Depending on the hydrogel scaffold materials and the structure, the properties of the crosslinked hydrogel can be engineered. Different prototyping techniques have been modified and tested for tissue engineering purposes mainly to produce soft tissue like scaffolds for cell encapsulation and delivery. (Billiet et al., 2012, Peltola et al., 2008)

4.1. Hydrogels

Hydrogels are polymeric materials containing vast amounts of water in their structure having gel like appearance. Due to this feature hydrogels have unique physical properties which are different from properties of the solvent and the polymer. Hydrogels can be engineered to resemble the extracellular matrix of various tissues which enable their use in medical applications such as biosensors, implants, cell-delivery and drug-delivery devices (Chaterji et al., 2007, Burdick and Prestwich, 2011). Hydrogels can be tailored with certain chemicals to modify their physical properties for better bioactivity in the targeted tissue. Tailoring, also known as derivatizations, can modify the hydrogel to be stimuli responsive. These so called “smart” hydrogels can be for example temperature, pH or UV crosslinkable thus enabling minimal invasive delivery methods or different gelation requirements. In particular, below the body temperature forming hydrogels have been extensively studied for drug delivery and tissue engineering purposes (Burdick and Murphy, 2012, Kim et al., 2005, Mortisen et al., 2010).

Thermoresponsive polymers will go through a reversible sol–gel transition when the lower critical solution temperature (LCST) is reached. In fact a small temperature change, usually between 3-5ºC, around the LCST makes the polymer chains to collapse and aggregate or to expand and unfold responding to the changes in hydrophobicity or hydrophilicity between the polymer chains and aqueous media. This behavior is illustrated in Figure 4.1 where the polymeric structure is presented under and over the LCST. When the hydrophilic equilibrium is shifted more towards hydrophobic balance by changing the temperature over LCST the binding affinity of the water molecules decreases and the polymer chains are open for chemical binding and entanglements. This property is the key feature concerning the use of the thermoresponsive polymers as

hydrogel scaffold materials in tissue engineering. (D'este et al. 2012; Malonne et al. 2005; Mortisen et al. 2010)

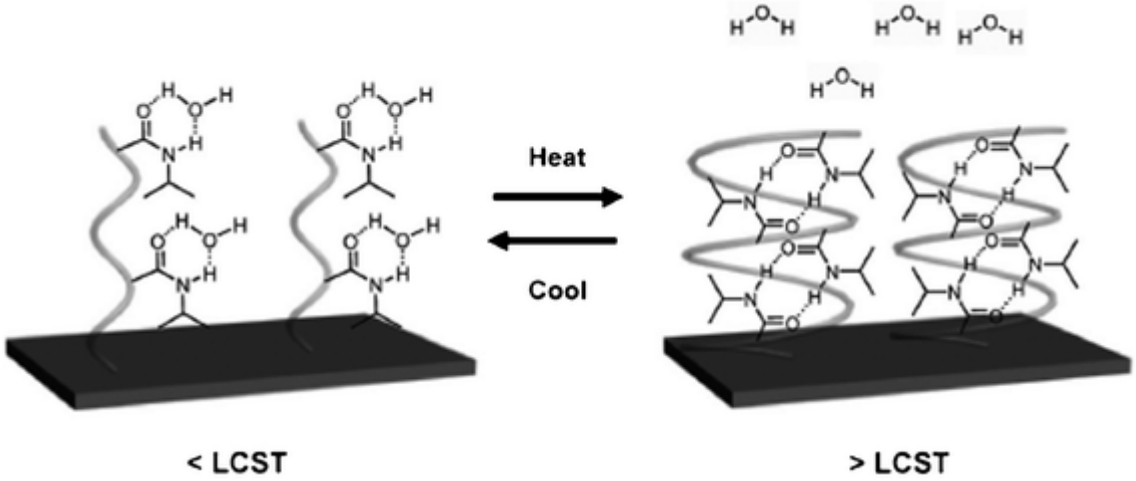

Figure 4.1. *Schematic illustration of reversible hydrogel formation in respect of temperature changes (Yamada et al. 1990).*

Photosensitive hydrogels can be crosslinked via visible light or UV light exposure in the presence of photoinitiator molecules. Photocrosslinkable hydrogels can be for example injected with the donor cells in vivo to the targeted tissue before crosslinking with UV light to ensure the hydrogel formation and implant attachment. These photosensitive hydrogels have been studied extensively due to their advantages in in vivo utilization and in highly controlled crosslinking (Lee et al. 2007; D'Arrigo et al. 2012; Fairbanks et al. 2009; Li et al. 2003). The controlled crosslinking can be initiated at room temperature or at physiological condition by brief exposure to UV light that initiates free radical polymerization. By changing the UV exposure time, photosensitive side groups or their grafting densities the hydrogel crosslinking can be tailored to yield optimized mechanical properties and degradation rates for the implant. Photosensitive side groups that have been grafted onto polymers include methacrylate (D'Arrigo et al. 2012; Bonino et al. 2011), acrylate (Lee et al. 2007) and vinyl groups just to name few. Photocrosslinkable hydrogels require the presence of photoinitiator in their crosslinking reaction. These initiators are toxic in high concentrations and more biocompatible are being developed. Fairbanks et al. compared I2959 (Ircacure®) and lithium phenyl-2,4,6-trimethylbenzoylphosphinate (LAP) photoinitiators in terms of required light wavelength in crosslinking and the cell viability after hydrogel UV exposure. They reported cell survival of encapsulated cells with LAP initiated crosslinking to be over 95% by UV light of 405 nm wavelength for 5 minutes (Fairbanks et al. 2009).

Functionalized polymers that react on alkaline or acidic changes by forming gel-like network crosslinking are called pH-sensitive polymers. These polymers contain acidic or alkaline functional groups in their polymer backbone. The pH changes close to the pK_a value of the functional groups will lead into an ionization of the group. This ionization will generate electrostatic repulsive forces leading to an increase in the hydrody-

namic volume (Chaterji et al. 2007). In hydrogels this means swelling and expanding. For the pH-sensitive hydrogels, the mobile ion concentration is important factor determine the magnitude of the predicted change. The degree of ionization of the functional groups acidic or alkaline will determine the swelling ratio and behavior of the hydrogel. (Chung and Park, 2009) The inner charge of the hydrogel relative to the external solution will cause water uptake (osmotic pressure), so that changes in solvent pH drive the volume change.

4.1.1. Hyaluronic acid poly(N-isopropylacrylamide)

Hyaluronic acid (HA), also known as hyaluronan, is a natural polysaccharide ubiquitous in almost all connective tissue. Hyaluronic acid has been extensively used in the biomedical applications such as dermal fillers and lubricants (ELEVESS™, Anika,; Hyalose; Ortholure™, Lifecore). HA can be found in high concentration in synovial fluid as well as in the articular cartilage structure where it functions as a lubricating substance. The structure of the HA disaccharide is illustrated in Figure 4.2. The carboxylic group and the hydroxyl groups are the main chemical functions used for the modification of HA. One HA disaccharide has the molecular weight (M_W) of 378 Da and it can be found in the body in sizes between few disaccharides to long molecular chains up 20 MDa.(Burdic et al. 2005; Stern et al. 2006)

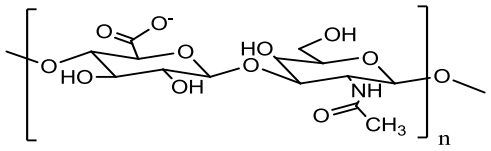

Hyaluronic acid

Figure 4.2. *Hyaluronic acid disaccharide structure is illustrated.*

The extensively studied biocompatible, thermoreversibel polymer poly(N-isopropylacrylamine) has a sharp gelation behavior below body temperature which makes it desirable material for the tissue engineering purposes. The PNIPAM has been grafted into several different biopolymers, natural and synthetic, to achieve biocompatible smart hydrogels (Li et al., 2011, Mortisen et al., 2010). Hydrogels derivatized by poly(N-isopropylacrylamine) (-PNIPAM) can be crosslinked by increasing temperature over 32°C which is a LCST for PNIPAM. This reversible crosslinking is a result from hydrophobic and hydrophilic interaction changes caused by the increased temperature. The hydrogen bonding between the polymer and water molecules becomes unstable when the temperature is increased. This results into bonding between the PNIPAM molecules and aggregation of the material. This transformation is making the hydrogels appearance changing from transparent to opaque (Zhang et al. 2008). The preliminary toxicity assessment was performed by (Malonne et al., 2005) to identify the toxic levels for PNIPAM. The results did not show any significant difference between the treated mice and the controls.

Hyaluronic acid poly(N-isopropylacrylamide) is a grafted structure of HA sensitive to temperature changes. HA-PNIPAM begins to self-aggregate after the reach of lower critical solution temperature (LCST). This phase transition happens in narrow temperature region above approximately 32°C. The degree of derivatization has a great influence on the final hydrogel properties which makes the controlled polymerization important firstly regarding mechanical stiffness and secondly regarding cell viability. (Seliktar, 2012)

4.1.2. Methacrylated biopolymers

Photocrosslinked HA hydrogels are typically being prepared using acrylates or methacrylates grafted to HA backbone that can be crosslinked via free radical polymerization. The preparation of the methacrylated derivative of hyaluronan and the polymerization reaction of methacrylated hyaluronic acid has been extensively investigated. (Chung, 2009; Masters et al. 2004; Burdick et al. 2005; Burdick and Prestwich, 2011) One of the simplest and widely used reaction for HA metacrylation is the reaction illustrated in Figure 4.3. (Smeds et al. 2001; Chung, 2009) This figure combines also the H^1-NMR spectrum from methacrylated HA to illustrate the connection between the polymer and H-NMR spectrum. Some important peaks (a-c) have been identified from the H-NMR spectrum. Peak a is referring to the methacrylate side chain two protons which are both resonating at their own peaks at 5.6ppm and 6.1ppm. Peak b belongs to the methyl group of methacrylate and the peak c 1.9ppm belongs to the methyl group of HA. When these peak integrals are then compared the grafting density can be easily calculated.

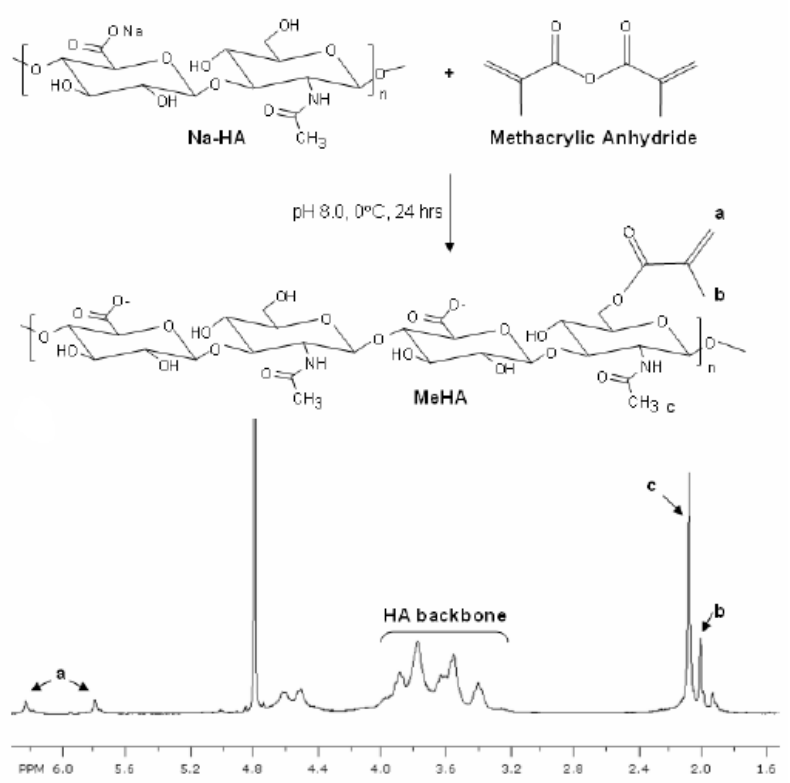

Figure 4.3. *Methacrylation reaction in schematic picture and ^{1}H-NMR spectra from MeHA. In NMR: a) methacrylate alkane protons each own peak, b) methacrylate methyl group, and c) HA methyl group. (Chung, 2009)*

Methacrylated hyaluronic acid is crosslinked by exposing it to UV light. This crosslinking reaction requires the use of a photoinitiator and exposure to certain wavelength of UV light that excites the initiator. These HA hydrogels are utilized for encapsulation of cells and drugs for use in biological therapies (Chung, 2009).

Chondroitin sulfate is composed of repeating disaccharide units of glucuronic acid and N-acetylgalactosamine with a sulfate group and a carboxyl group on each disaccharide (Li et al. 2003). Chondroitin sulfate is a biopolymer that is present in cartilage and it is part of the aggrecan molecule responsible for lubrication on the surface. It binds to a polymer chain with keratin sulfate and brushes out from the core protein to give aggrecan its well known shape (Fosang et al., 1992). We used chondroitin sulfate to enhance the biological nature of the bioinks because chondroitin sulfate is a major component of the cartilage ECM. Both chondroitin sulfate and dextran can be easily methacrylated by following similar grafting reaction illustrated in Figure 4.3. (Li et al., 2003).

4.2. Rapid prototyping techniques

Several prototyping techniques for hydrogel-based tissue engineering have been developed in past decades. Rapid prototyping consists of computer controlled material deposition performed in layer-by-layer fabrication. These precise RP techniques enable defined 3D implant manufacturing for tissue engineering. With these techniques 3D scaf-

folds can be produced in complex shapes, micrometer scales and reproducible (Ferris et al. 2013; Gauvin et al. 2012; Turunen et al. 2011). The computer interface allows predetermined scaffold designing which can be further connected with computed tomography (CT) or magnetic resonance imaging scans taken from the desired implantation site (Hollister, 2005). Thus, these techniques ensure optimal fitting for patient's needs and customized properties for each implant. Figure 4.4 illustrates the three main branches of rapid prototyping. The most interesting and promising techniques are explained in this chapter.

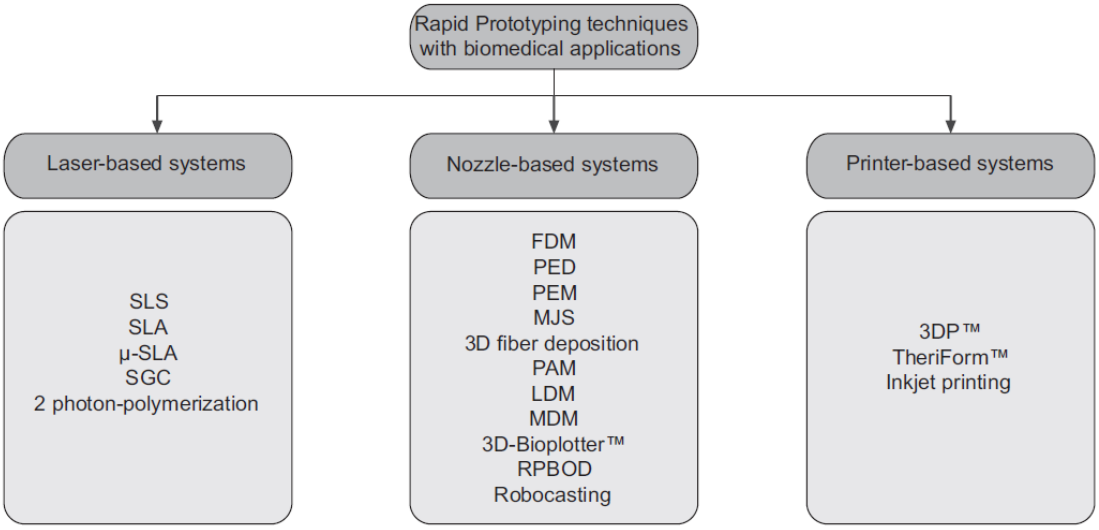

Figure 4.4. *Illustration of rapid prototyping techniques investigated in medical field (Billiet et al. 2012).*

4.2.1. Laser-based systems

Stereolitography (SLA) and **micro-stereolithography** (μ-SLA) are both employed in hydrogel rapid prototyping. The only difference of these RP techniques is the resolution of the technique in which the conventional SLA can reach as low as 30 μm and μ-SLA as low as 1 μm. An SLA device consists of a UV-light source that can be maneuvered in horizontal plane, a reservoir of desired material and a manufacturing stage that can be maneuvered in vertical plane. In SLA manufacturing usually a laser light is focused on the surface of the material reservoir and desired 2D pattern is exposed to a laser. The working principle is that a lasers exposure excites the photoinitiator that initiates the crosslinking reaction. Crosslinked 2D layer structures can be either lowered (bottom-up) or lifted up (top-down) with the manufacturing platform to produce the final 3D structure (Billiet et al. 2012). When comparing these two approaches the biggest differences are the light source positioning on top or under the material reservoir, photocrosslinking exposure to oxygen on bottom-up and always smooth exposure surface in top-down. To ensure the attachment of the layers the platform is moved a smaller distance than the exposure depth of the laser. Post processing treatments are additionally required for removing excess uncrosslinked material around the 3D structure and usually further UV curing is needed to produce the final stiffness and uniting of the structure. Two addi-

tional improvements have been developed for faster SLA scaffold production 1) Digital micro-mirror device™ (DMD) and 2) Solid ground curing (SGC). The DMD is basically a set of mirrors that can be individually programmed to reflect the UV light from one source to project the entire 2D pattern. This addition will reduce the manufacturing time substantially and it makes bigger scaffold production feasible. The SGC technology is also designed for reducing the scaffold production time by allowing the 2D layer structures to be exposed at once. This is done by an additional photomask created on site that allows the UV exposure only through the transparent areas. (Billiet et al. 2012; Turunen et al. 2011; Peltola et al. 2008; Gauvin et al. 2012)

Two photon-polymerization (2PP) is a fine laser patterning technique capable of micron scale resolution and features less than 100 nm in 3D. A 2PP technique is a patterning tool rather than large scale scaffold production technique. It can pattern the structure into the photosensitive material itself by moving the focus point of the lasers. The working principle is that the two lasers working with near-infrared femtosecond laser pulses of 800 nm are focused in a single point designated to be crosslinked. In the focus point, the photoinitiator absorbs simultaneously two photons at 800 nm wavelength which enables the photons to act as a photon of 400 nm wavelength that initiates the crosslinking. (Billiet et al. 2012; Peltola et al. 2008)

Laser-based RP techniques suffer from limitations such as need for photo crosslinkable materials, presence of cytotoxic photoinitiators and UV exposure to the cells. Furthermore, at the moment SLA techniques require a substantial reservoir of material and the use of fast reacting photoinitiators in high concentrations. The two photon-polymerization technique is only feasible in patterning since it would require too much time to produce actual scaffolds. Additionally, patterning in a material requires photoinitiators for 2PP to be used with the initiators for the additional crosslinking if it is desired. (Turunen et al. 2011; Billiet et al. 2012)

4.2.2. Nozzle-based systems

Four different nozzle types have been used in different nozzle-based RP techniques 1) pressure-actuated, 2) solenoid-actuated, 3) piezoelectric and 4) volume-actuated nozzles. All the nozzle-based systems are dependent on material viscosity, patterning speed, nozzle diameter and pressure. These parameters alternate the produced line thickness and width. Increasing the pressure in the nozzle will increase material deposition and line diameter. However, by increasing patterning speed or material viscosity the line diameter can be kept the same or even decreased. All of these variants have an effect in the final construct resolution. (Billiet et al. 2012)

Pressure-assisted microsyringe (PAM) technique consists of a 5-20 μm pneumatic glass capillary syringe dispensing material in vertical plane and a manufacturing stage that moves in X and Y planes relative to syringe. Nozzle sizes of few micrometers can-

not extrude particles such as cells without introducing shear stresses high enough to tear up the cell membranes and sacrificing the integrity of the cells. (Billiet et al. 2012)

Low-temperature deposition modeling (LDM) technique requires usage of temperatures below 0ºC to solidify the extruded material. In this system the nozzle moves in horizontal plane depositing material to the degraded temperature stage capable of moving in vertical axis. More advanced version of the technique is called multiple nozzle low-temperature deposition modeling (M-LDM) which can extrude several different materials simultaneously to cut down the production time of the scaffold. This also enables composite structures to be extruded in one session (Billiet et al.2012; Hollister, 2005).

3D-Bioplotter™ has a unique feature to pattern a viscous material into a liquid medium with corresponding density. This feature works especially in favor for low viscosity materials and fragile scaffold structures before curing. 3D-Bioplotter is a simple system where the nozzle is able to move in all X, Y and Z axis while the manufacturing stage is stationary. This property enables straight plotting into well plates or such. This plotting technique can be used for either continuous dispensing of single lines or dispensing of micro sized droplets. Dispensing of the plotter is based on pneumatic nozzle by applying pressurized air for wanted extrusion volume to guarantee homogeneous droplet volumes. Compared to technologies using lowered or elevated temperatures this dispensing technology enables the usage of thermosensitive materials or cells. (Billiet et al. 2012; Peltola et al. 2008)

Robocasting technique is a common name for RP of ceramic slurry 3D structures by using robotics. Materials deposited with this technique are ceramic slurries containing up to 65% ceramics in powder form. Contrary to 3D-Bioplotter, the robocasting is based on moving manufacturing stage (x, y, z) and fixed nozzle position. When the high viscous slurries are dispensed on the moving stage they require some special rheological features including shear thinning properties but also fast solidification to prevent flow after dispensing. This RP technique is reliant of sufficient materials and it is only applicable for slurries. (Billiet et al. 2012)

Direct ink writing (DIW) is a RP technique based on colloidal, high viscous, inks. This technique is highly dependent on the inks used in the patterning process since the layers are directly dispensed on top of the previous one. The direct ink writer consists of vertically moving dispensing nozzle that can have multiple syringes attached and a horizontally moved manufacturing stage. (Turunen et al. 2011; Billiet et al. 2012)

Extrusion/aspiration patterning (EASP) technique is clever RP system capable of switching between extrusion and aspiration continuously. Actually three different phases can be identified from this system: extrusion, aspiration and refilling. Extrusion is

controlled with a closed valve that guides compressed air into the nozzle whereas by opening the valve will guide air pressure out of the system aspirating the desired amount of the material by Bernoulli suction. Then the valve is closed again and the empty space is refilled. By cycling these phases the 3D object is created. (Billiet et al. 2012)

4.2.3. Printer-based systems

Printers can be divided into continuous injection or drop-on-demand techniques. In continuous injection the air pressure is used to inject droplets continuously whereas in drop on demand technique the individual drop size and timing can be optimized. In inkjet printers the air jet breaks the droplets into tens to hundreds of micron sizes droplets that are guided on the substrate. This layer by layer printing will further establish the 3D structure. (Ferris et al. 2013)

3D Printing™ technology is a solid state RP technique compatible with hydrogels. 3D Printing consists of reservoir of material from which the new layer is added to the printing chamber, the printing chamber where the actual printing takes place and an inkjet print head. The whole printing process is divided into three steps: in the first step a powder layer is spread over the printing stage. In the second step the printing of liquid binder fuses the powder together and forms a 2D layer. In the third step the printing stage is lowered one layer distance and reservoir is lifted likewise. When the cycle is repeated the 3D structure starts to form. The liquid binder either dissolves the particles for fusion or swells them for interpenetration. In polymer hydrogels the polymer chains of each layer entangle and bond via inter-diffusion. Most interestingly the powders can consist of single powder, mixed powders or even blended polymer powders. Furthermore, powder particles can be surface coated or multilayered. After the printing process the 3D structure is reveled and purified from the excess powder. The binder is the crucial component of this technique and it has to full fill several requirements such as high concentration of binder but low viscosity for jetting, biocompatibility even in high concentrations and fast reaction with the powder to enable fast printing cycles. (Murphy et al. 2013; Billiet et al. 2012)

Inkjet printing technology is a common name used from all the liquid phase inkjet technologies. The printer itself can follow the 3D printing construct where powder reservoir is just replaced with a liquid one or the direct 3D inkjet writing where the printing creates the 3D layered structure. In inkjet printing the ink can be jetted, meaning srayed with high pressure on the surface. (Ferris et al. 2013; Billiet et al. 2012)

4.3. Requirements for bioinks

Bioprinting, a subgroup of rapid prototyping, is a printer based technique dispensing droplets using a magnetig microvalve. Bioprinting requires the development of specified printing materials, bioinks. The bioinks are mixtures of biocompatible materials

from synthetic or natural sources that can be combined with the fibers, particles or even cells. The bioink composition and properties should mimic the natural ECM in the desired implantation site or tissue. By providing a natural like or superior engineered ECM for the cells will effect significantly on the binding affinity of the cells and furthermore on the proliferation. The optimal bioink is a balance between four requirements: handling, printability, biocompatibility and mechanical properties after printing illustrated in Figure 4.5. The handling, printing and biocompatibility of the ink should be always kept the highest possible regardless of the desired tissue. The handling is an important requirement for the bioink since they have to be homogeneous mixtures and easily useable. The inks can be mixed with the cells and biological cues such as growth factors. Handling is also important for the transition to the clinics where the easy handling and efficiency are respected high.(Murphy et al. 2013)

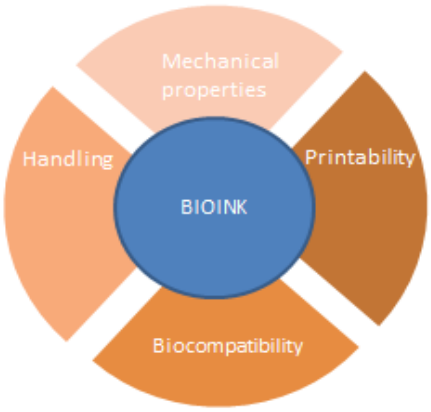

Figure 4.5. *The four requirements from the bioink.*

The printability of the ink has to be considered in order to produce scaffolds or grafts by using the bioprinting technologies. In order to print high viscous inks, shear thinning behavior is required to decrease the shear forces in the needle. Also the fast gelling is required immediately after the printing to retain the printing resolution. If the printing parameters are incorrect the resolution can be lost even if the ink would have been suitable for the printing. Too high pressure or feeding rate compared to dispenser speed will increase the line dimensions and the resolution is lost. The mechanical properties of the ink refers to printability, however, the mechanical properties of the hydrogel construct can be significantly influenced by changing the ink composition and further enhanced with 3D structure and printing parameters. The increase of the modulus during the tandem gelation is illustrated in Figure 4.6. Mechanical properties should resemble the native cartilage in order to provide sufficient environment and support for the chondrogenesis.

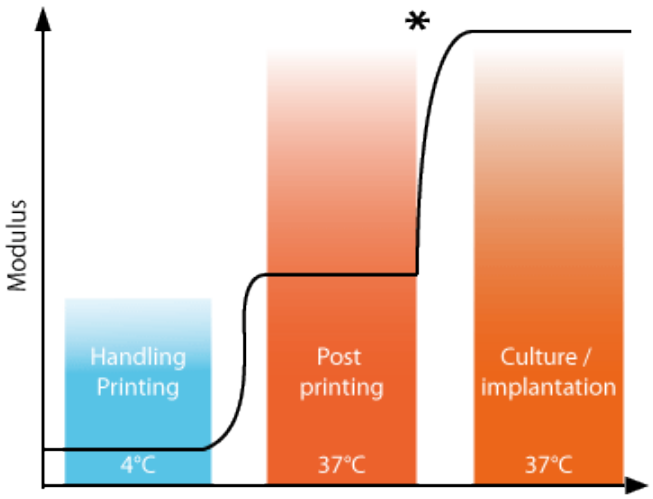

Figure 4.6. *Theoretical illustration of the desired behavior in tandem crosslinked bioinks.The line illustrates the growth of the modulus and the star symbol (*) marks the point of UV exposure.*

The bioink composition can affect both the crosslinking behavior and crosslinking method. Temperature crosslinking is an effective gelation method in printing techniques; due to small volumes the temperature shift is almost immediate. However, the temperature crosslinking does not provide enough stability for in vivo implantation due to lack of covalent crosslinks. Hence, the photosensitive crosslinking is providing an increased modulus and stabile structures for the construct. (Billiet et al. 2012; Lee et al. 2007)

5. MATERIALS AND METHODS

HA Sodium salt (HANa) from *Streptococcus equi* was purchased from Contipro Biotech s.r.o. (Czech Republic). Two different M_W batches were used:

• High M_W fraction (HM_W), with weight-average molecular weight M_w = 1506 kDa and polydispersion index M_w/M_n = 1.53, where M_n indicates the number-average molecular weight.

• Low M_W fraction (LM_W), with M_w = 293 kDa and M_w/M_n = 1.86.

Amine terminated poly(N-isopropylacrylamine) (NH_2-PNIPAM), synthesized in AO Research Institute Davos, was received with number-average molecular weight M_n = 24 kDa and polydispersion index M_w/M_n = 1.7. This compound was grafted onto HM_W hyaluronic acid. Methacrylated dextran (DEXMA) and methacrylated chondroitin sulfate (CSMA) were received from INNOVENT Technologieentwicklung Jena (Germany). DEXMA M_W = 15-20 kDa and the degree of methacrylation was 0.76 (0.76 out of 4 available groups were functionalized, equals 19%). Chondroitin sulfate methacrylate CSMA was approximately 20 kDa in M_W with a degree of substitution with methacrylates being 0.18 (4.5%) and 0.9 (22.5%) for sulfates. Methacrylated hyaluronic acid (HAMA) was produced in house from LM_W hyaluronic acid. Table 5.1 summarizes all the materials details.

Table 5.1 *Used materials with their abbreviations, molecular weight of the polymers and the grafting densities.*

Polymer	**-PNIPAM**	**Methacrylation**	**M_W**	**Grafting density**
Hyaluronic acid (Thermoresponsive)	**(HA PNIPAM)**		**1506 kDa,**	**(4.6%)**
Hyaluronic acid		**(HAMA)**	**293 kDa**	**(35.5%)**
Chondroitin sulfate		**(CSMA)**	**20 kDa**	**(4.5%)**
Dextran		**(DEXMA)**	**15-20 kDa**	**(19%)**

Lithium phenyl-2,4,6-trimethylbenzoylphosphinate was used in all the photoinitiation reactions and it was purchased from INNOVENT Technologieentwicklung Jena (Ger-

many). Other chemicals such as NaOH, HCl, methacrylic anhydride, acetone and ethanol were all of analytical grade and purchased from Sigma-Aldrich.

5.1. Materials synthesis and polymerization

Synthesized materials for the thesis were HA-PNIPAM and methacrylated HA. Both synthesis protocols and techniques are explained further in this chapter.

5.1.1. Synthesis of HA-PNIPAM

High molecular weight HANa was transformed into its tetrabutylammonium salt (HA-TBA) via cationic exchange according to established procedures (Bellini & Topai, 2000). At room temperature, 2.0 g of HATBA were dissolved in 200 ml of dimethyl sulfoxide. The activation reaction to obtain the acyl-imidazole was performed by addition of methanesulfonic acid and 1.1-carbonyldiimidazole, both equimolar to the repeating unit of HA. Following 1 h of stirring, 3.7 g of amino-terminated PNIPAM were added and stirred at room temperature. The derivatization reaction is illustrated in Figure . In the prehydrolyzed batches, 0.1% (v/v) of water was added just before the amino-terminated polymer addition. After two days, 10% (v/v) of saturated NaBr was slowly poured into the reaction solution and stirred 1 h before dialysis against demineralized water using regenerated cellulose dialysis tubes with nominal M_W cut-off 50 kDa (Spectrapor no. 6, 34 mm flat width) for five days. Products were freeze-dried, desiccated under vacuum at 42°C and stored at room temperature.

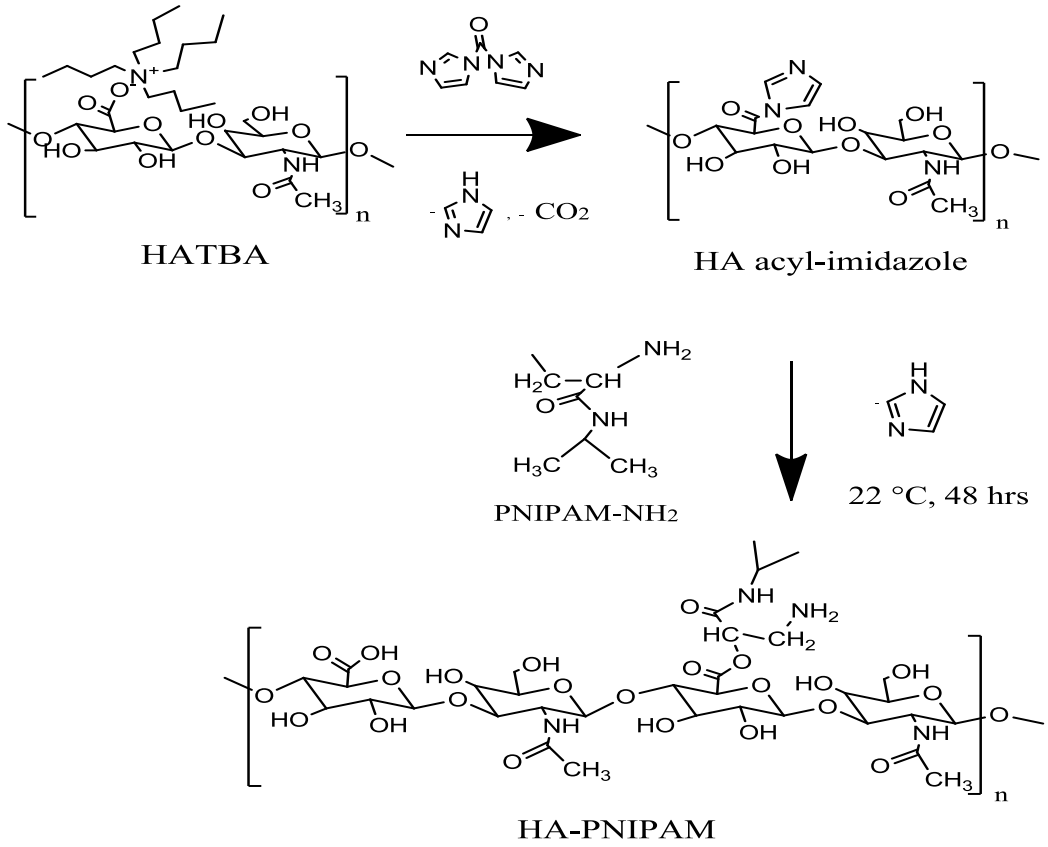

Figure 5.1. *Derivatization reaction for grafting HA-PNIPAM.*

5.1.2. Synthesis of methacrylated hyaluronic acid

Low molecular weight HA was methacrylated using methacrylic anhydride and click chemistry. This reaction chemistry is illustrated in Figure 5.2.. HA was dissolved in deionized water to produce a 1.5 w/v % solution. This solution was stirred overnight before adjusting the pH to 8 by adding 1N sodium hydroxide (NaOH). Then, 20 fold excess of methacrylic anhydride was added and the reaction was allowed to proceed in an ice bath (~0°C) for 24h. Due to methacrylic acid formation in the reaction the pH required constant maintenance over the reaction time. First three hours of reaction the pH was balanced at 8 by adding 5M NaOH drop wise. After 24h the methacrylate hyaluronic acid solution was precipitated into an excess of ethanol and the precipitate was collected by vacuum filtration. The dried precipitate was rehydrated into its original sample volume by deionized water and dialyzed for three days against deionized water using a dialysis membrane (Spectralpor® M_w cut off 12-14 kDa). The deionized water was changed every 24h. Products were freeze-dried and stored at room temperature.

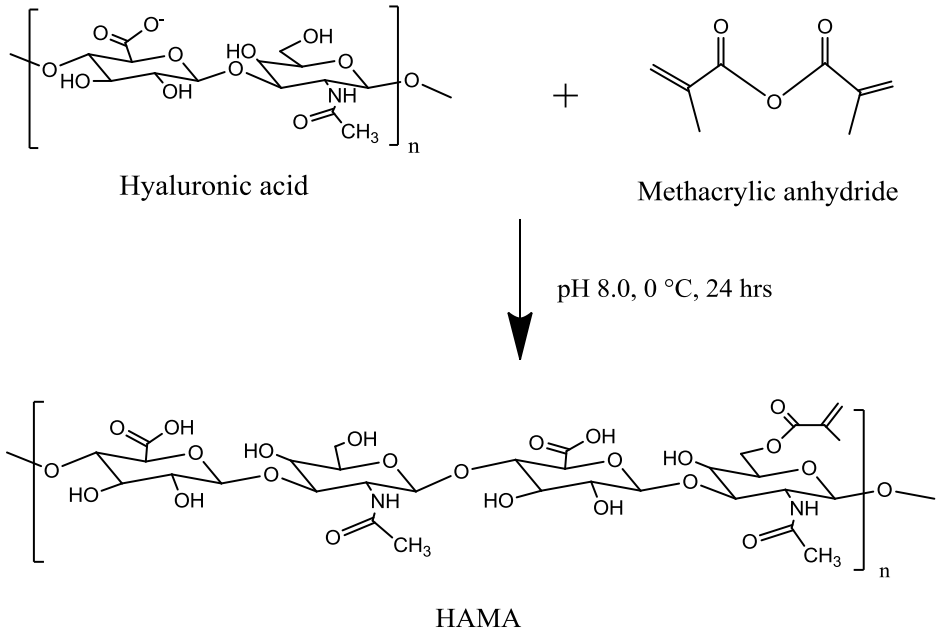

Figure 5.2. *Derivatization reaction for grafting methacrylated hyaluronan.*

The methacrylation reaction requires basic conditions for the reaction to continue. Indeed, due to methacrylic acid production during the reaction, the pH drops fast under pH 8 which prevents further grafting of the methacrylate. Furthermore, when the reaction pH increases over pH 10 the degradation of HA begins, degrading the M_W of the final product and increasing the polydispersity.

5.2. Chondrocyte isolation and encapsulation

Chondrocytes were harvested from a fresh bovine knee joint purchased from the local slaughter house. Using sterile techniques, the knee joint was dissected and thin slices of articular cartilage were harvested into 50 ml of sterile isolation medium containing dulbecco's modified eagle medium (DMEM) (Invitrogen 32430) with Anti-Anti 1%. An approximate amount of 3 g of cartilage was harvested from the bovine knee in each isolation. Figure 5.3 illustrates the articular cartilage harvest sites and as seen only thin slices of cartilage were harvested to prevent contaminations from blood cells and osteoblasts. Cartilage slices were washed twice with fresh medium before the two step digestion was started. The first digestion step consists of adding sterile filtered pronase enzyme digestion solution, containing 4 mg/ml pronase enzyme (Sigma) in isolation medium, on the cartilage isolation dish. The amount of 6ml for each gram of cartilage was used. The digestion was carried out in an incubator (37ºC) under gentle stirring for two hours. After the first digestion step the slices were washed with fresh medium three times. The second digestion step, collagenase digestion, was mediated with collagenase enzyme (type II sigma 546 U/mg) used in concentration of 0.6 mg/ml in the isolation medium. This collagen digestion solution was added in volume of 6 ml for each gram of cartilage and let react in an incubator (37ºC) under gentle stirring for six hours. The

digested cartilage was further filtered through a 100 μm cell strainer sieve followed by another filtration with 20-40 μm cell strainer sieve. After the last filtration the solution was centrifuged to obtain a cell pellet. The cell pellet was dissolved into cell cryostorage medium and aliquoted into cryotubes before freezing to -80°C at a concentration of $1.5x10^6$ cells/ml.

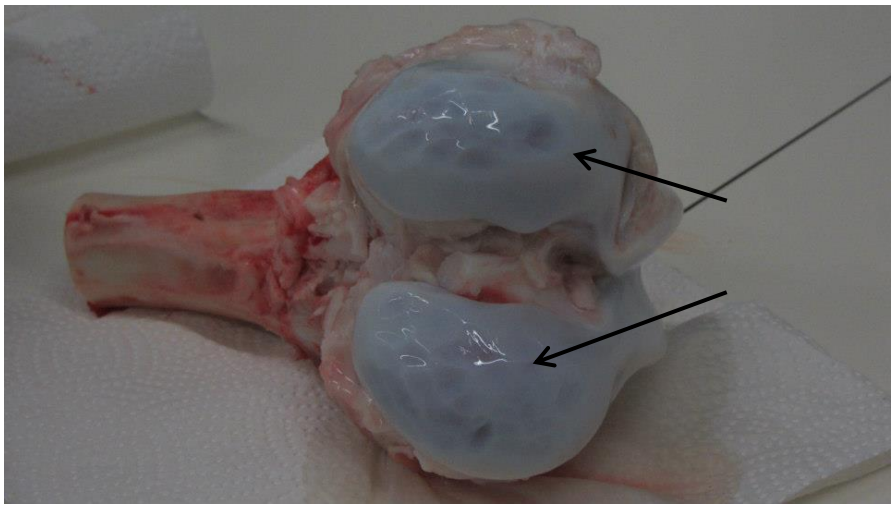

Figure 5.3. *Bovine lower limb after collection of articular cartilage.*

UV crosslinking of methacrylated biopolymers were conducted either with an external UV lamp, the UV source in the rheometer or the UV source in the bioprinter. LAP was always used as photoinitiator at 0.05 w/v % which has been found to be efficient and biocompatible (Fairbanks et al. 2009). The external UV lamp (Blak-Ray® B-100AP, UVP LLC, USA) was performing at a 365 nm wavelength and 100 watt power. This external UV lamp was used to produce hydrogels 10mm in diameter and 1.5mm in height with Q-gel disc caster 1.5 (Q gel SA, Switzerland). Other UV sources were used during the usage of the rheometer or the bioprinter. During the bioprinting the UV curing was performed with the UVPEN-365, emitting 365 nm wavelength UV light, in 150 mW power illuminating the scaffold construct stationary from the center.

Hydrogels were produced for the cell encapsulation and viability assays as follows: Bovine chondrocytes ($6x10^6$/ml) were suspended in 20 µl bovine chondrocyte medium (bCh medium). The bCh medium consisted of Dulbecco's modified Eagle's medium (DMEM; Invitrogen 32430) supplemented with 10% fetal bovine serum, 1% Anti-Anti and 50µg/mL of ascorbic acid prepared in sterile conditions. Furthermore, this bCh medium was mixed with 130µL of each material combinations including 0.05% LAP and pipetted onto Q-gel disc caster 1.5 for hydrogel disc formation. Tandem gelation was initiated in an incubator (37°C) for 15 minutes until stabile temperature was achieved and further crosslinked with 5 minute UV- light exposure. The final hydrogels were transferred into 24-well plates and incubated in chondrocyte culture medium for 1 and 7 days.

Cell encapsulation for bioprinting happened as similar as possible to the previously described hydrogel cell encapsulation. Shortly, the bioinks were mixed with chondrocytes (6million/mL) and 0.05% (v/v) LAP prior to printing onto a heated (37-40ºC) printing stage. The heating enabled the rapid encapsulation of the cells and stiffening of the structure for the printing of the layered construct. After every other layer the construct was exposed to UV for 30-40 seconds to ensure stabile hydrogel formation.

5.3. Characterization

5.3.1. NMR analysis

Nuclear magnetic resonance (^{1}H-NMR) measurements were performed for all the synthesized materials in order to determine the degree of derivatization and possible residues of toxic substances after dialysis. Samples for nuclear magnetic resonance measurements were prepared from lyophilized samples. Approximately 15-20 mg of dried sample was dissolved into approximately 1 ml of deuterium oxide (D_2O). The solution was stirred several hours before collection into NMR tubes. ^{1}H-NMR analysis was performed on a Bruker Avance AV- 500 NMR spectrometer using deuterium oxide as solvent without residual HOD peak suppression. Spectra were calibrated using 3- (trimethylsilyl)-1-propanesulfonic acid sodium salt as chemical shift internal standard, and processed with Mestrenova software.

5.3.2. Rheology

Rheological measurements were performed to determine important material features such as crosslinking kinetics, flow behaviors and recovery rate. Rheological measurements were performed with an Anton Paar rheometer MCR 301 equipped with a peltier element and UV curing system. Measurements were performed with a plate-cone setup (CP50-1) with diameter of 50mm and angle of 1° for the liquid samples. For measuring pre cross-linked gels, a plate-plate setup with a PP10 plate with diameter of 10mm was used. The zero gap distance was calibrated before each measurement to ensure accurate positioning of the probe. Additionally, to avoid drying of the samples, a solvent trap was filled with a sufficient amount of Milli-Q-water. All the samples were dissolved to the desired concentration in phosphate buffer saline (PBS) pH=7.4 to mimic physiological conditions.

5.3.3. Cell viability

Cell viabilities inside the photoencapsulated hydrogels were assessed with two microscopes: 1) transmission microscope and 2) fluorescence microscope.
The transmission microscope Zeiss, AXIO Vert. A1 was used in assessing the morphology changes of the cells and their distribution in the hydrogel. Furthermore, the hydrogels structures appearances were analyzed.

The fluorescence microscope Zeiss, AXIO Observer Z1 with ApoTome.2 was used for the cell viability assays. ApoTome camera (MRm) and XLmulti S1 temperature incubator were used in thermoresponsive hydrogel analysis during the temperature increasing.

The cell viability assays were performed with a live/dead assay kit (LIVE/DEAD® Invitrogen). Hydrogels were first washed with warm PBS for two times to wash away all the excess substances that could possibly interfere with the dyes. Then for each examined hydrogel 500 µl of live /dead dye was prepared. Dye consisted 0.5 µl of calcein AM and 2 µl of ethidium homodimer in each milliliter of PBS. Calcein AM is cleaved by esterases inside the cell membrane in live cells to yield cytoplasmic green fluorescence and cell membrane impermeable ethidium homodimer labels nucleic acids of the cell nucleus with red fluorescence. If the cell membrane is intact ethidium homodimer cannot penetrate into the nucleus and the cell is emitting only 500-550 nm green wavelengths.

ZEN pro 2011 software was used in for image aquisition. Calcein AM imaging was done with the reflector 38 HE green fluorescent protein with an excitation wavelength 450-490 nm and an emission wavelength of 500-550 nm divided by the beam splitter in 495 nm. Ethidium homodimer imaging was done with the reflector 43 HE DsRed with an excitation wavelength 538-562 nm and an emission wavelength of 570-640 nm divided by the beam splitter in 570 nm. DAPI imaging was done with a reflector 49 DAPI with an excitation wavelength 335-383 nm and an emission wavelength 420-470 nm divided by the beam splitter in 395 nm.

All the cell viability images were processed by using FIJI software for cell counting. Separate live and dead images were counted and the viability was counted by using following equation:

$$(1)\quad \frac{Live}{Live + Dead} \times 100\% = Viability\ \%$$

, where the viability percentage represents the whole gel. For each viability determination, three identical hydrogels were produced and cultured. Each of the gels was imagined in 3-5 different locations which were then counted and averaged.

5.4. Bioprinting

Bioprinting of hydrogel constructs was performed with the Bio Factory® (Regen HU Ltd, Switzerland) shown in Figure 5.4. This 3D manufacturing instrument based on the solenoid valve technology has eight upgradable work stations allowing bioprinting with variable bioinks. Each bioink is loaded into individual syringes mounted onto the station and connected to a compression air hose providing pressure. The biosafety cabinet guarantees sterile processing conditions with HEPA H14-filtration and UVC high effi-

ciency emitter for disinfection. An electromagnetic jet printhead CF-300N equipped with a needle of 300µm diameter was used in all the printing experiments. The UV curing was performed with the UVPEN-365, emitting UV light at a wavelength of 365 nm, with 150 mW power.

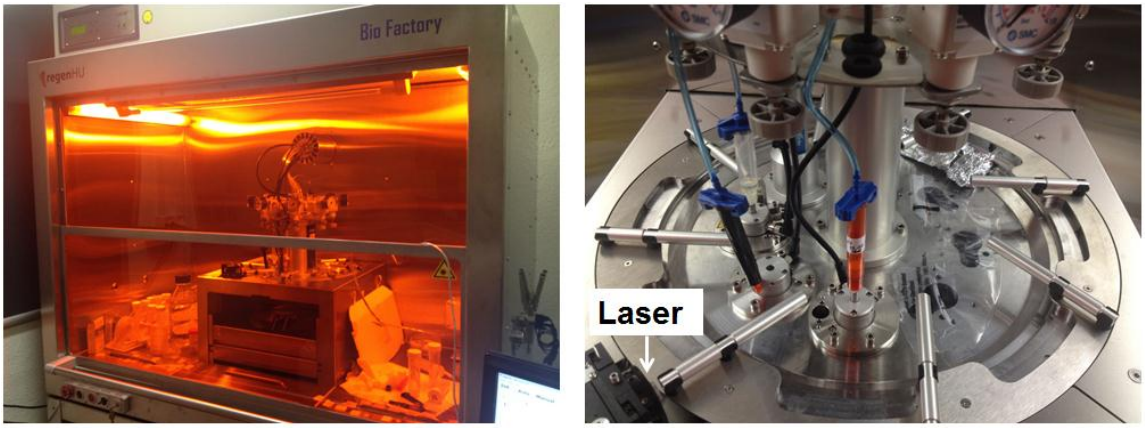

Figure 5.4. *BioFactory® bioprinter was used in all the printing experiments. The printing equipment is completely inside the laminar flow hood enabling sterile working environment. Laser source suitable for UV crosslinking is illustrated in the picture on the right.*

Bioprinting was done by drop-on-demand printing in which the solenoid valve allows individual droplets to be printed. The droplet size and frequency can be optimized by simultaneously varying syringe pressure, valve opening time, closing time and frequency. The manufacturing stage was moving in the X, Y, Z – axis while the dispenser station was changing the bioinks when required. Printing was done over dual glass plate with a heating unit attached to enable controlled substrate temperature. UV light was always applied at the mid position of the structure to ensure uniform exposure.

Computational designs of the structures were drawn with the BioCAD designing software produced by Regen HU Ltd. The drawings were then translated into ISO code to be processable by the bioprinter.

6. RESULTS & DISCUSSION

Results and discussion will follow the predetermined idea of investigating the rheology of the materials before moving into the biology point of view. In the biology section, the focus is set on the cell viability and morphology. Based on the both investigations, the optimal bioink compositions were chosen and tested for printing. The final step was to produce a 3D scaffold that would mimic the layered structure of the native articular cartilage. All the concentration % values given are in w/v% in the result section.

6.1. Hydrogels optimization

6.1.1. Polymers

Hydrogen NMR was performed for the HA-PNIPAM and HAMA polymers synthesized for this thesis. This was carried out to determinate the grafting density of the materials and to control the process of polymerization. These results could be further compared to the new batches produced in order to ensure uniform material properties.

H^1-NMR spectra from the HAMA polymer is illustrated in Figure 6.1. Two peaks on the left at 6.1 ppm and 5.6 ppm are referring to the two protons in the methacrylate side chain (Figure 4.3.). The wide peak section in the middle of the spectrum is referring to the polymer backbone of HA. This wide section contains peaks from ten protons between 3.0 ppm - 4.1 ppm and due to these over lapping peaks it is not accurate to use them the grafting density calculations. The peak at 1.9 ppm on the right refers to the methyl group of HA which contains three protons and is used as a reference to calculate the grafting density. The peak at 4.8 ppm is the water peak caused by the hydrogenation of deuterium oxide used as a solvent in NMR measurement.

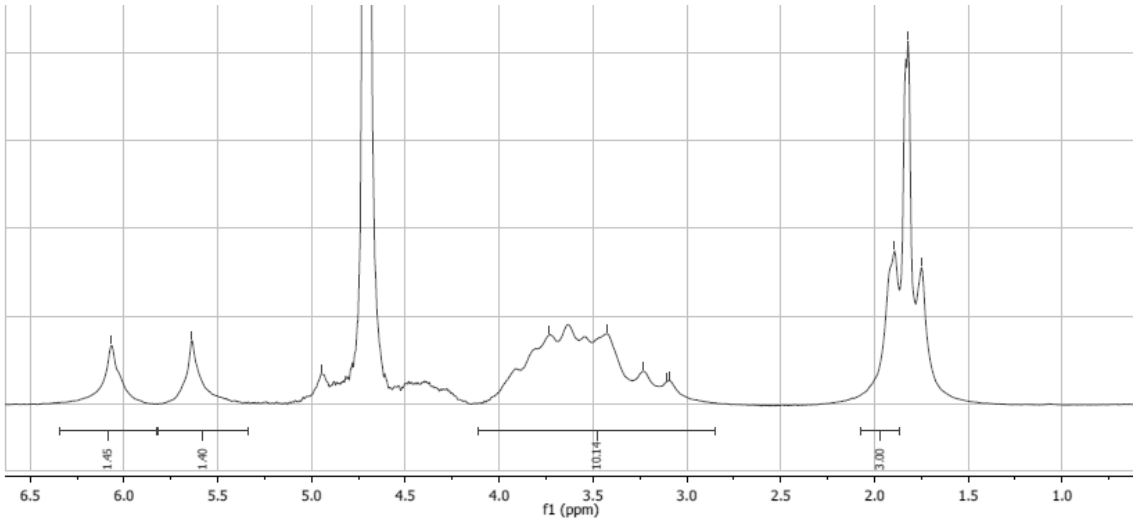

Figure 6.1. *H-NMR spectrum from methacrylated hyaluronic acid. Certain important integrals over the peak areas are marked in the figure.*

The grafting density of HAMA was calculated from the ratio of the relative peak integrations of the methacrylate proton 5.6ppm or 6.1ppm (Figure 4.3.) to the HA methyl group in 1.9ppm. The equation used for the calculation of the grafting density was:

(2) $$\left(\frac{\int 5.6ppm}{1\ proton}/4\right) X\ 100\% = Grafting\ \%$$

, where the integral over 5.6ppm is the area of 1.4 in Figure 6.1 and four refers to the four hydroxyl groups in one repeating unit of hyaluronic acid.

First the integral over 5.6 ppm peak was normalized to the integral of the HA methyl group peak at 1.9 ppm which has three protons. Without this normalization the result would not represent the true value of grafting density. This value is then divided by one proton in the representative peak. The quotient is further divided by four which comes from the total value of possible grafting places in one repeating unit of HA. This result was converted into percentages by multiplying by 100%. The grafting density in our case gave us 35% grafting which is a relatively high value.

Figure 6.2 illustrates the H^1-NMR spectrum from HA-PNIPAM. When comparing the Figure 6.1 and Figure 6.2 it is clear that the peaks referring to HA backbone (3.0 ppm - 4.1 ppm) and methyl group (1.9 ppm) are both present and at the same position in both spectrums. Because of the complex PNIPAM side chain the grafting density calculations require more understanding of the structure.

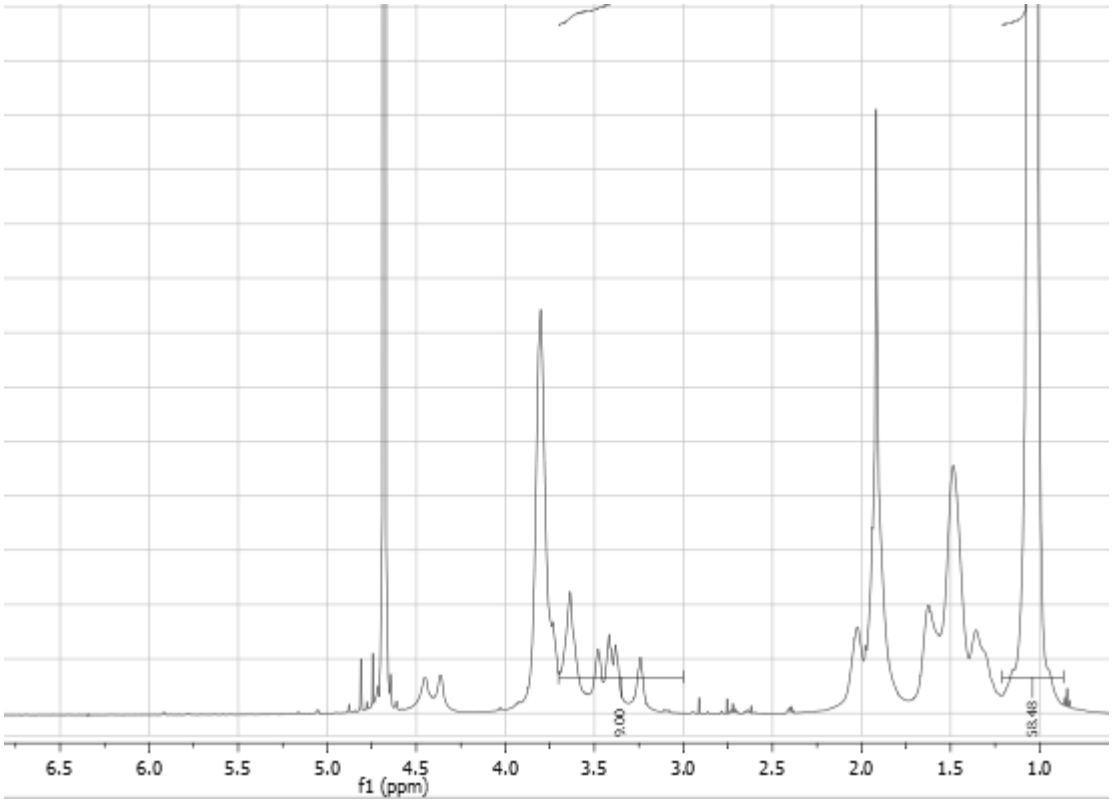

Figure 6.2. *H-NMR spectrum from hyaluronic acid grafted with PNIPAM. Integral of HA backbone and the –PNIPAM side chain are marked in the figure.*

The grafting density of HA-PNIPAM was calculated according to a previously established technique (D'Este et al., 2012). The density is retrieved from the ratio between the relative peak integrations of the PNIPAM side chain protons (peak at 1.1 ppm) and the HA backbone between 3.0 – 3.7 ppm. This wide overlapping area has nine protons which are used for normalization. The HA methyl group peak at 1.9 ppm cannot be used for normalization since it interferes with PNIPAM group. The equation used was:

$$(3)\quad \frac{PNIPAM\ chain\ Mw}{PNIPAM\ monomer\ Mw}\ X\ 6\ protons = Tot.protons$$

$$(4)\quad \frac{\int 1.14ppm}{Tot.protons} X\ 100\% = \ Grafting\ \%$$

, where the total protons refers to the PNIPAM side chain protons and M_w represents the molecular weight.

First the total amount of PNIPAM protons is calculated by dividing the PNIPAM M_w, in our case 24kDa, by the PNIPAM monomer M_w which is 113.16 Da. This value is equal to the number of repeating monomers in the PNIPAM side chain and it has to be multiplied by the six sp^2-hybridized protons in the structure. These protons are the origin of the 1.14ppm peak (D'Este et al., 2012). After the number of total protons of the PNIPAM chain was calculated, the integral over the 1.14 ppm peak was divided by the

number of total protons similarly as in HAMA equation. This result was translated into percentages by multiplying the value with 100%. The grafting density calculated was 4.6% which was slightly inferior to the values achieved with the same synthesis method (D'Este et al., 2012).

6.1.2. Thermoresponsive component

Hyaluronic acid was grafted with –PNIPAM side chains and prepared in three different concentrations to study the kinetics of the temperature crosslinking. Figure 6.3 illustrates the rheology data received from these three concentrations during the temperature increase under oscillation. The three concentrations were HA-PNIPAM 10%, 15% and 20% from which the HA-PNIPAM 15% was hypothesized to provide the best properties. The LCST was determined from the point when storage modulus G' equals to loss modulus G''. In general, when the temperature was increased over the LCST the loss modulus increased up to 5 orders of magnitude with these materials. As illustrated in Figure 6.3 the 10 % solution has narrow crosslinking regime (2 fold increase within 5°C), similarly to 15% solution (3 fold increase within 4°C). However, the final modulus of the HA-PNIPAM 10% is approximately 1.5 magnitudes lower which results in inadequate properties for layered bioprinting. The monolayer printed from HA-PNIPAM 10% did not give enough structural support for the next layer and the printed construct did not grow in height. On contrary, the HA-PNIPAM 20% solution had the highest final modulus and it gave enough structural support for the layer printing. However, the crosslinking kinetics was slowed down due to the higher polymer concentration and increased viscosity. Even the increased number of aggregating sites in the polymer backbone did not increase the crosslinking kinetics. Thus, aggregation begins at lower temperature when the PNIPAM chains were coiling and entangling between the HA chains. Furthermore, the initially higher polymer concentration increases the liquid viscosity for one order of magnitude compared to the other concentrations 10% and 15%. Based on these measurements and the additional experiments the HA-PNIPAM 15% was chosen to be blended with the biopolymers.

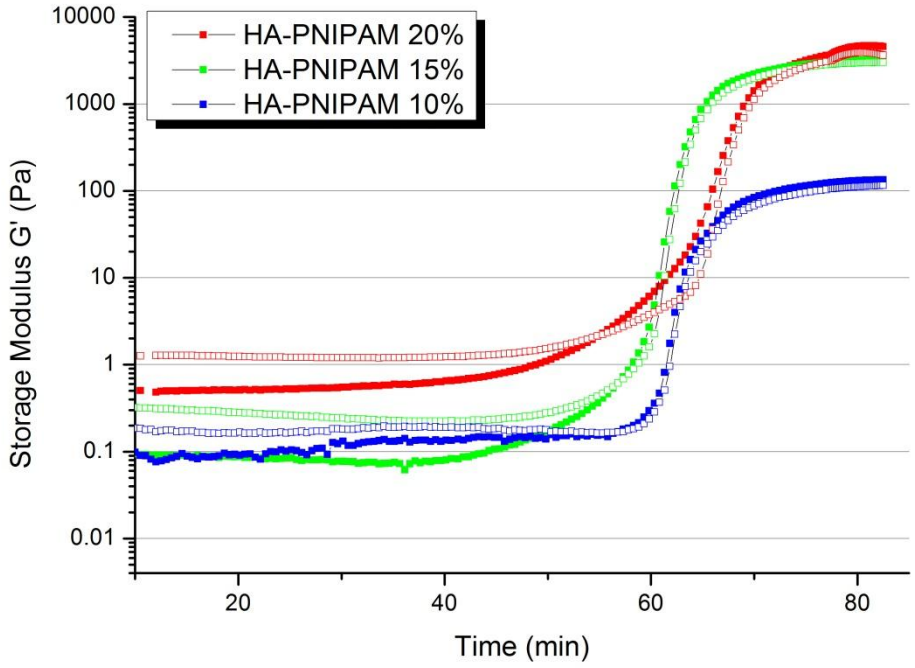

Figure 6.3. *HA-PNIPAM was temperature cross-linked by increasing the temperature by 0.5°C/min. Closed symbols represent the G' and open symbols G'' (loss modulus).*

HA-PNIPAM temperature crosslinking is a reversible crosslinking process which means the modulus achieved after the gelation should return back to its original when the temperature is back to its initial value. Additionally, this should happen at the same rate in order to be considered total reversible crosslinking. As illustrated in Figure 6.4, the thermoresponsive crosslinking did not return along the same curve and, most importantly, it did not return to the initial viscosity value. The crosslinking temperature was found to be 31.1ºC (LCST) when the sample was heated, but in cooling the opening of the crosslinks happened at significantly lower temperatures. However, the exact disentanglement point is hard to determine. These results are contratictory to the ones previously described in literature (D'Este et al., 2012). This difference can result from different measuring techniques. The hermetic pan of thermal gravimetric analysis (TGA) can prevent the water escaping more efficiently than the rheometer's peltier element covered with an inert seal in combination with the solvent trap. However, the TGA measurement is measuring total energy used in heating (heat flow) and cooling which does not tell anything about the mechanical properties after the polymer heating. These results from HA-PNIPAM 15% solution prove the temperature crosslinking to be partially irreversible, where some polymer entanglements exist after the cooling. These entanglements will increase the viscosity if material handling and storage are not performed at temperatures below 27 ºC.

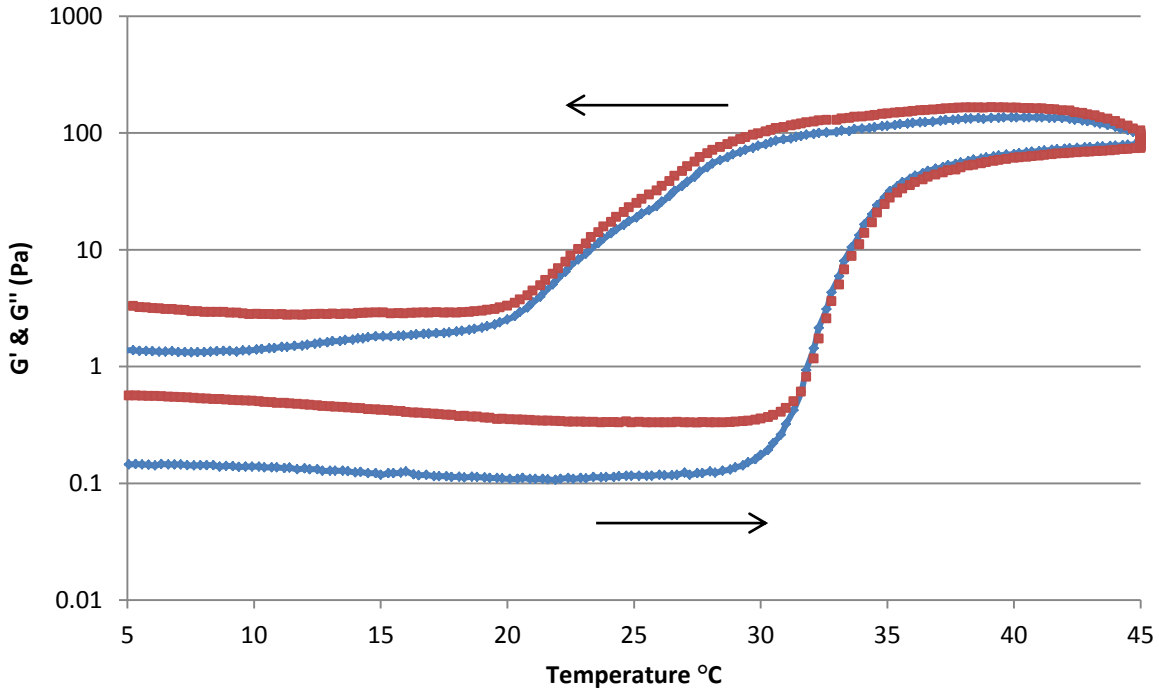

Figure 6.4. *HA-PNIPAM 15% heating and cooling cycle. Red symbols represent the G'' (loss modulus) and blue symbols the G' (storage modulus) The arrows illustrate the direction of the temperature change. Both heating and cooling were increased 0.5ºC/min.*

Recovery test for HA-PNIPAM 15% solution was done to understand the effect of shearing the sample during the printing. The measuring cone CP50-1 was rotated at the shear rate of 100 s^{-1} for one second before returning to oscillation mode measuring G' and G''. The recovery curves were normalized for easier comparison due to high viscosity differences from sol state in 4°C to gel state in 37°C. As illustrated in Figure 6.5, the recovery rate in 4°C was 100% compared to 37°C where the recovery was neglectable. Interestingly, already at 27°C, the recovery rate reduced to approximately 50%. These results reveal that a controlled printing environment is necessary in order to maximize the post-printing thermoresponsive effect of the ink. These results clarify the networking crosslinking of HA-PNIPAM which cannot reorganize after the network rupture.

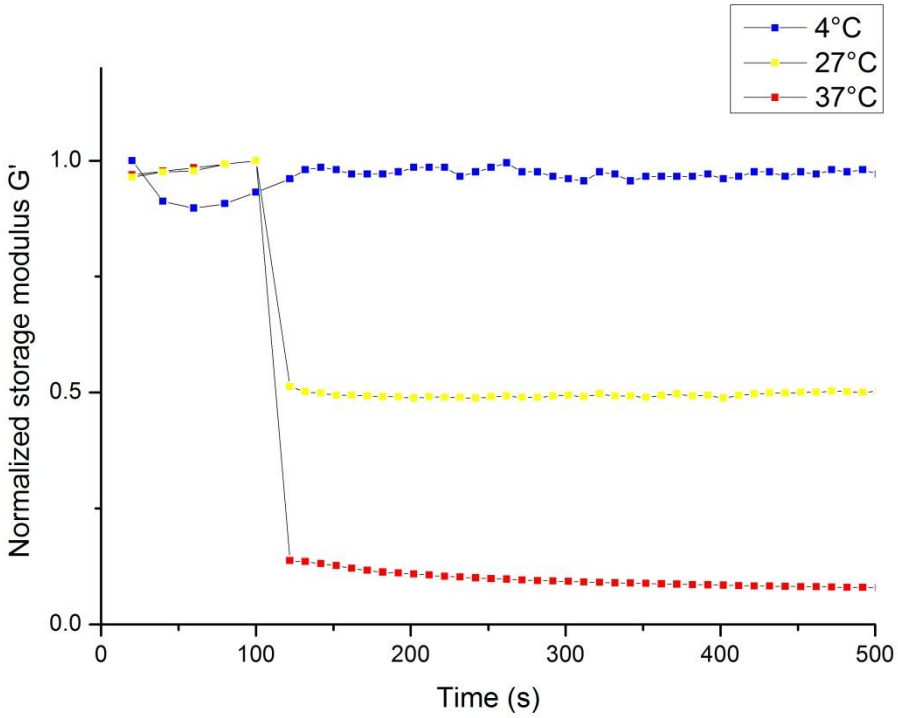

Figure 6.5. *Recovery test was performed for HA-PNIPAM 15% solution and the normalized results are presented.*

The HA-PNIPAM 15% solution has the best properties for the different concentrations of HA-PNIPAM for desired bioinks regarding crosslinking kinetics, initial viscosity and reversibility. The low initial viscosity is related to PNIPAM interactions preventing the HA chains from interacting.

6.1.3. Tandem crosslinking

Tandem crosslinking was analyzed from HA-PNIPAM 15% blended with all three biopolymers in several concentrations. Rheology measurements were performed for all the blends following the same procedure: First a five minutes waiting time ensured the equilibrium of the measuring system with the sample. In a second step, the temperature was increased 0.5ºC/min between 4 ºC and 45 ºC. After, the temperature was kept constant at 45 ºC for five minutes. This was followed by decreasing the temperature to 37 ºC before UV exposure, subsequently UV exposing the sample for 5 minutes and then keeping the temperature at constant 37 ºC without UV exposure to see the final modulus stability.

Methacrylated chondroitin sulfate was blended with HA-PNIPAM 15% solution in concentrations between 3 to 10%. CSMA1% blend did not UV crosslink so the measurements were started from 3% blends. As illustrated in Figure 6.6, the temperature crosslinking region is not altered even with biopolymer blending except in CSMA 10% blend which lacks a temperature gelation transition. This might be caused by the electrostatic interactions with positively charged PNIPAM chains so that those cannot interact and

entangle. Increasing the temperature decreases the viscosity until the PNIPAM starts to coil and aggregate releasing water molecules from its structure. The modulus starts to increase after LCST but CSMA molecules prevent the HA-PNIPAM chain entanglement and PNIPAM bridging. Same interactions affects in the CSMA 3% and 5% blends preventing high degree of temperature crosslinking. However, tandem crosslinking is dependent on the two inversely proportional crosslinking processes. The UV crosslinking is proportional to the methacrylated polymer concentration in all blends. High crosslinking density after temperature increase would prevent methacrylated polymer and initiator movement leaving UV crosslinking low. Due to interactions of the sulphate groups in the CSMA with the PNIPAM chains, the UV crosslinking is the dominating crosslinking process, enabling a high modulus of the final construct.

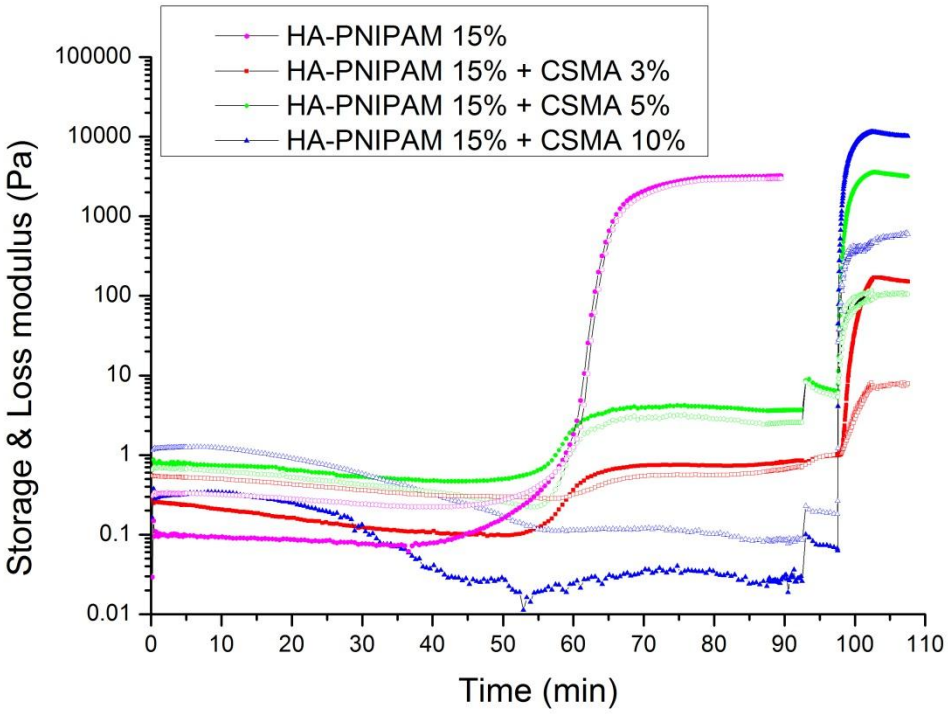

Figure 6.6. *Methacrylated chondroitin sulfate blends at different concentrations. Closed symbols represent the G' and open symbols G'' (loss modulus). The storage moduli for the blends were for the CSMA10% 11.5 kPa, 5% 3.6 kPa and 3% 0.2 kPa. Tandem crosslinking behavior was further compared to pure HA-PNIPAM 15% crosslinking.*

Tandem crosslinking of methacrylated dextran blends were performed similar to the CSMA blends. Figure 6.7 illustrates the modulus concentration dependency of the DEXMA blends in tandem crosslinking. Initial viscosities of the blends were at the same level. For the dextran blends, temperature crosslinking is occurring in the same regime as pure HA-PNIPAM 15% and the modulus increases to similar orders of magnitudes. However, the dense crosslinking network disabled the UV crosslinking of DEXMA 3% and DEXMA 5% which are not able to further crosslink the samples. Only the DEXMA 10% blend was crosslinking due to high concentration of methacrylate groups.

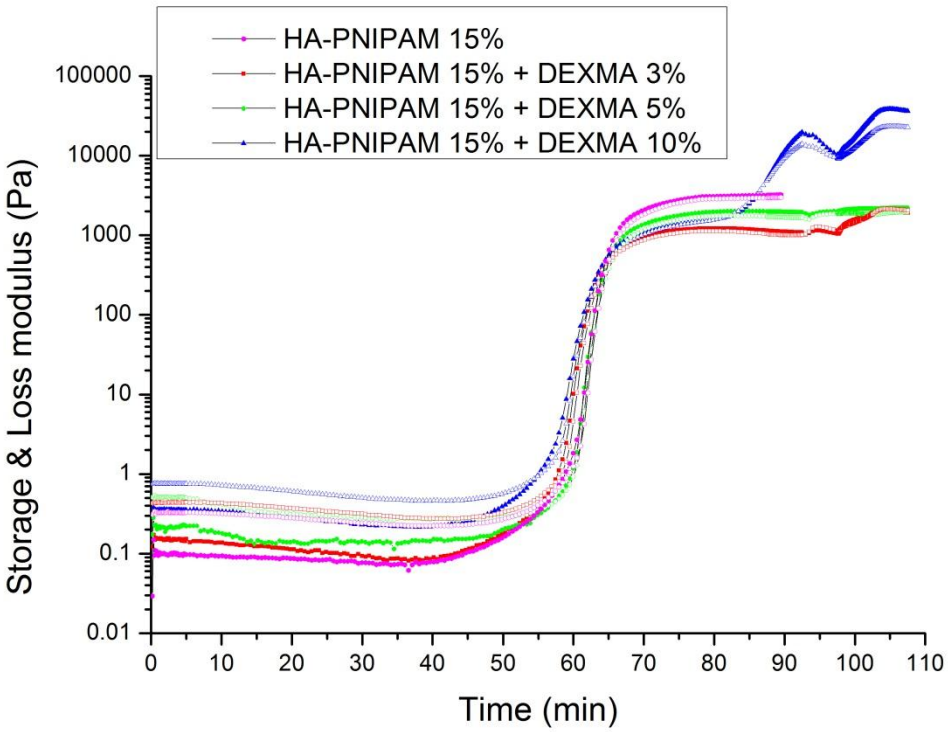

Figure 6.7. *Methacrylated dextran blends at different concentrations. Closed symbols represent the G' and open symbols G'' (loss modulus). The storage moduli for the blends were for the DEXMA10% 38.5 kPa, 5% 2.2 kPa and 3% 2.1 kPa. Tandem crosslinking behavior was further compared to pure HA-PNIPAM 15% crosslinking.*

Methacrylated hyaluronic acid blends moduli were approximately two folds higher than in the other biopolymer blends due to the M_W of HA (293 kDa). Higher concentrations than HAMA 3% were impossible to mix with the HA-PNIPAM 15% and load into the bioprinter syringes so those were excluded from the measurements. Methacrylated HA was blended in at the concentrations of 1% and 3% as illustrated in Figure 6.8. The HAMA 1% blend has the lower initial viscosity so it can temperature crosslink further than HAMA 3% blend. Although, the HAMA 1% blend's modulus remains lower in the end as expected due to the smaller concentration of methacrylate groups. Compared to other analyzed polymer blends the HAMA 3% and HAMA 1% had the highest storage modulus values 8.4 kPa and 5.5 kPa respectively.

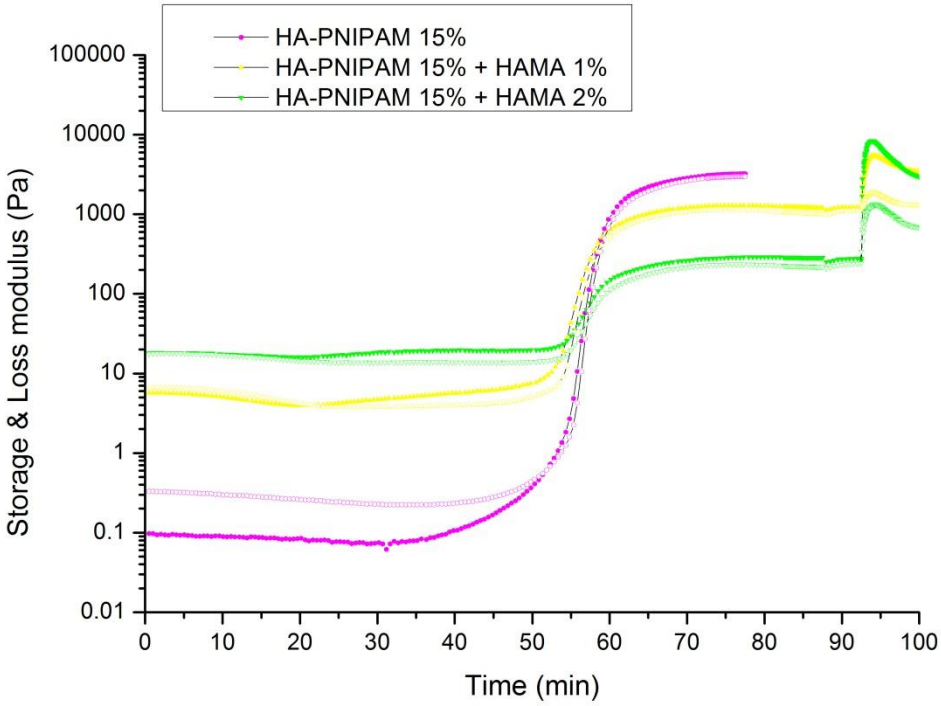

Figure 6.8. *Methacrylated hyaluronic acid blends in different concentrations. Closed symbols represent the G' and open symbols G'' (loss modulus). Tandem crosslinking behavior was further compared to pure HA-PNIPAM 15% crosslinking.*

Three promising bioinks were mixed with the cells and the influence of the addition of cells to the bioinks on the tandem crosslinking process was analyzed. Figure 6.9 illustrates the bioink changes when 6 million bovine chondrocytes were mixed into the inks. The temperature crosslinking region is not altered by cells, which was one critical aspect to study to make sure the inks are still biologically printable. However, the modulus increase during the temperature gelation process was significantly decreased in all inks due to cells preventing the entanglement of the polymer chains and PNIPAM molecules to assemble. This effect was significantly present in DEXMA based ink where the difference was higher than two orders of magnitude. This could be explained by an increased initial viscosity. In the other two inks the initial viscosity merely influenced by cell mixing.

The photoinitiated UV crosslinking behavior is a rapid reaction initiated immediately upon UV exposure. Cell mixing does not have an influence on the storage modulus after printing in HAMA 1% and CSMA 5% solutions. Both bioinks achieved the same storage and loss modulus values with or without the cells. Also the lower thermoresponsive crosslinking with the cells did not have any effect. This inversely proportional tandem crosslinking behavior of the bioinks can be identified easily from these gels, however, the behavior of the dextran based solution was unexpected. It had significantly lower storage modulus after both crosslinkings despite the complementing effect of photocrosslinking.

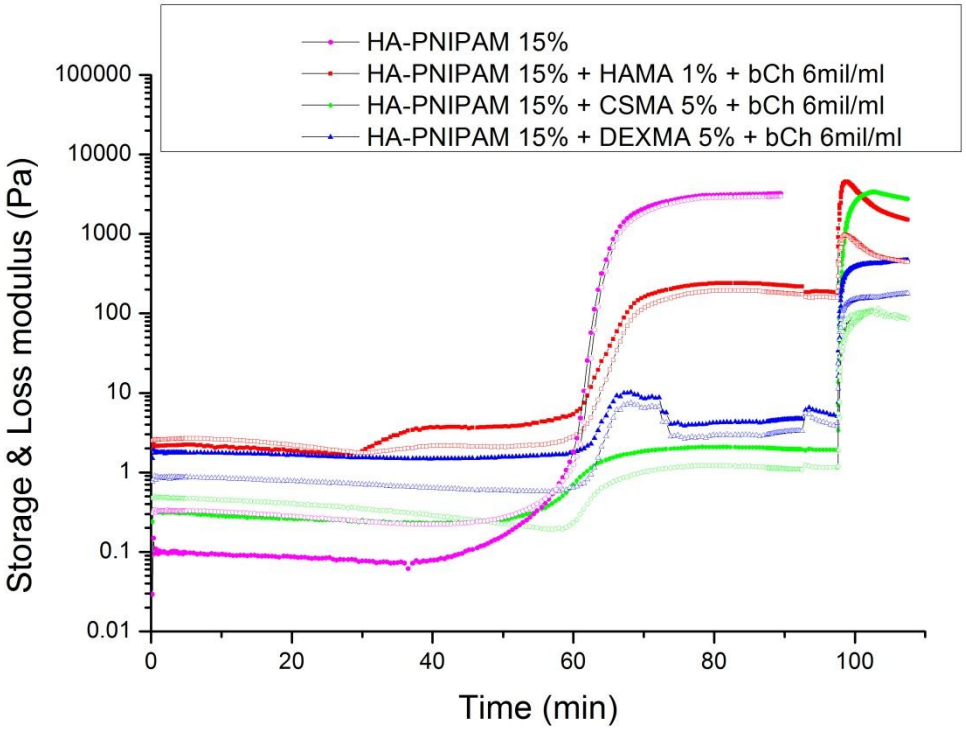

Figure 6.9. *Promising bioinks mixed with cells to study cells effects on tandem gelation. Closed symbols represent the G' and open symbols G'' (loss modulus).*

Based on all the previous rheology measurements and analysis, three bioink compositions were chosen for the 3D layered cartilage structure printing. The exact arrangement of the thermo- and photosensitive crosslinking is illustrated in Figure 6.10. The highest storage and loss modulus are achieved with these inks from our tested materials. However these G' and G'' values have to be further enhanced to achieve native cartilage properties.

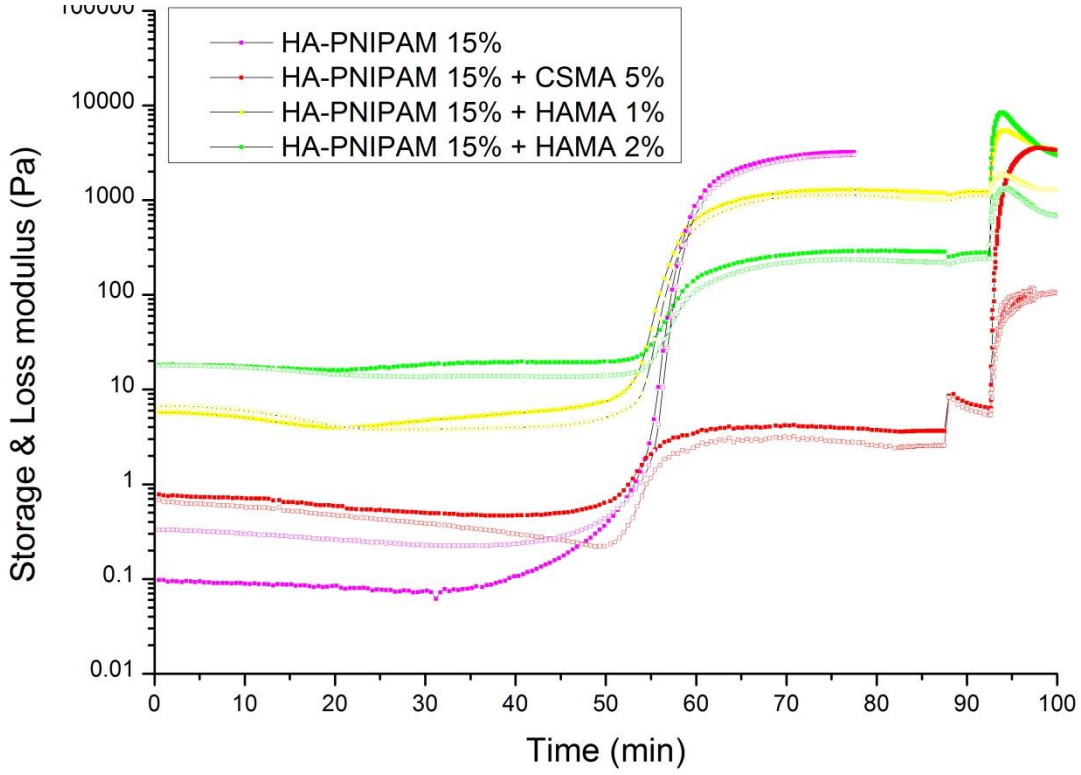

Figure 6.10. *Three chosen bioink combinations and their tandem crosslinking profiles. Closed symbols represent the G' and open symbols G'' (loss modulus).*

Rheology of the bioinks was the most intensive investigation for the desired mechanical properties. The chosen hydrogel compositions were the toughest tested but they still lack far behind the native cartilage storage and loss modulus 50.1 MPa ± 12.5 MPa and 4.8 MPa ± 1.0 MPa respectively (Fulcher et al., 2009). This issue is the common problem for hydrogel based scaffolds which cannot be utilized into load bearing applications.

6.2. Photoencapsulation of chondrocytes *in vitro* study

Chondrocytes residing in the articular cartilage ECM are under hypoxia in avascularized tissue. Chondrocytes are unable to proliferate further and their appearance is rounded due to complete encapsulation into ECM (Temenoff and Mikos, 2000). The Figure 6.11 illustrates how the chondrocytes interact with the biological cues of the bioinks. Morphologies of the chondrocytes are spread the most in images A and D and the least in image E. This behavior could be related to the higher stiffness in the HAMA 1% gel (Figure 6.11E) compared to other gels investigated. Rounded cells are more isolated and native chondrocyte like, however, the production of collagen II and other ECM molecules was not investigated from these gels. Stiffer gels have the downside to have a too dense network structure for sufficient nutrient transport which can lead to apoptosis of the cells. Cells in softer gels had more space to interact and elongate which can further shift the phenotype towards other cell types rather than chondrocytes.

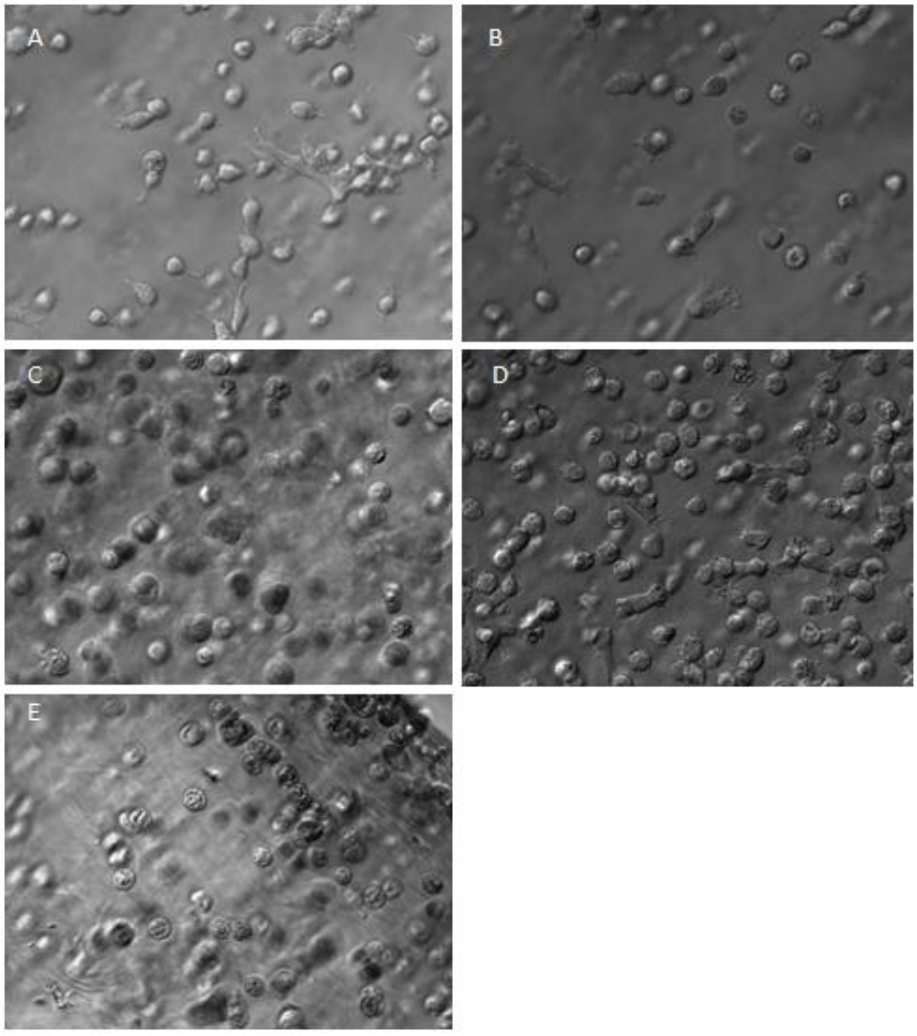

Figure 6.11 *Chondrocytes encapsulated in biopolymer gels after one day. Image A CSMA 3%, B CSMA 5%, C DEXMA 3%, D DEXMA 5% and HAMA 1%.*

Based on morphological differences it is impossible to say which gels provided the best surroundings for the cultured chondrocytes. Further histological analysis should be conducted to identify the produced ECM markers like collagen II and GAG's.

6.2.1. Cell viability

Cell viability assays were conducted for biopolymer gels and bioink gels to identify the biocompatibility with the chondrocytes. Figure 6.12 illustrates the cell viabilities imaged after one day and one week of culture. The softest gels, CSMA 3% and DEXMA 3%, were not able to support and encapsulate chondrocytes effectively which resulted in leaching out of chondrocytes. Furthermore, the CSMA 3% gel degraded and ruptured into several pieces which prevented the cell viability analysis from the gel. In both gels the significant drop in cell viabilities were recorded. Stiffer gels CSMA 5%, DEXMA 5% and HAMA 1% had promising viability values over 80% after seven days of culturing. The stiffness of HAMA 1% was almost double compared to the other stiffer gels.

Thus, HAMA produced the best cell viability values and it gave rounded shape for the chondrocytes as analyzed before (Figure 6.11).

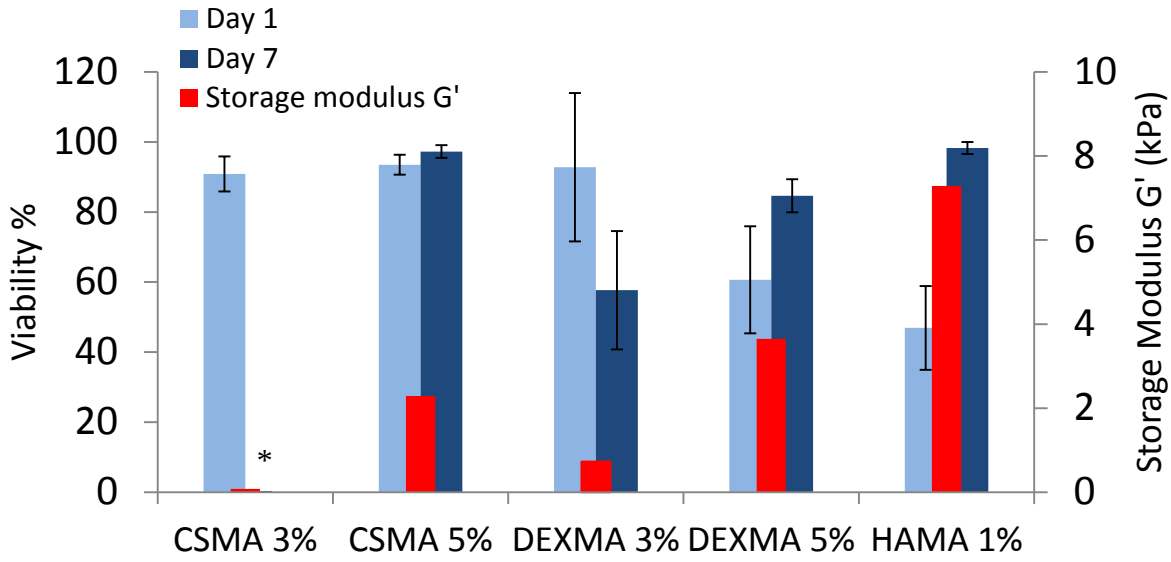

Figure 6.12. *Cell viability assay for biopolymer gels. Assays were conducted on day one and seven for three identical gels and the results were averaged. Error bars are marked in the figure and star symbol in CSMA 3% 7 day measurement that gels dissolved.*

Cell viability assays from the bioink gels were analyzed but higher than 100% viabilities were recorded after one day. After careful investigation the HA-PNIPAM auto-fluorescent effect was discovered. When the HA-PNIPAM is kept colder than the LCST, it is transparent liquid that can be imaged easily. However, when the temperature is increased to body temperature (> LCST), the PNIPAM aggregates start to appear in the fluorescent image. Furthermore, these particles were auto-fluorescent in both green and red channel which made cell viability calculations impossible from the bioinks. In future the (3-(4,5-dimethylthiazol-2-yl)-2,5-diphenyltetrazolium bromide (MTT) or/and histological analysis could be conducted to these gels to compare the cell viabilities. In MTT analyses the (3-(4,5-dimethylthiazol-2-yl)-2,5-diphenyltetrazolium bromide, which is a yellow tetrazole, is converted into purple formazan by living cells. After dissolving the transformed formazan the spectrophotometer such as plate reader is used to analyze the absorbance. Received data is not quantitative but it can be used to compare which material had more live cells.

6.3. Bioprinting with chosen bioinks

Bioprinting was the main development point in the third stage. Bioprinter parameters such as pressure, manufacturing stage moving speed, needle height, valve opening/closing time and valve frequency were adjusted to fit in each bioink. This stage is extremely time consuming which is one of the drawbacks in printer based rapid prototyping techniques. However, once the parameters have been set up for the standardized bioink the parameters do not require further adjustments.

6.3.1. Structures and resolution

Bioprinting was conducted with the 300 μm in diameter needle on a heated substrate (39ºC). The first printed bioinks were HA-PNIPAM 15% + HAMA 1% and HAMA 2% illustrated in Figure 6.13. As shown in Figure 6.13A, the line height and thickness after four 300 μm lines are approximately 1.0mm which means the ink had some flow after printing. This behavior is emphasized in the construct B where the line height and thickness are 0.9 mm and 1.4 mm, respectively. The resolution could be improved by decreasing the syringe pressure or increasing the printing speed. Furthermore, faster crosslinking kinetics of the bioink would enable layers to be printed directly on top of each other without flow.

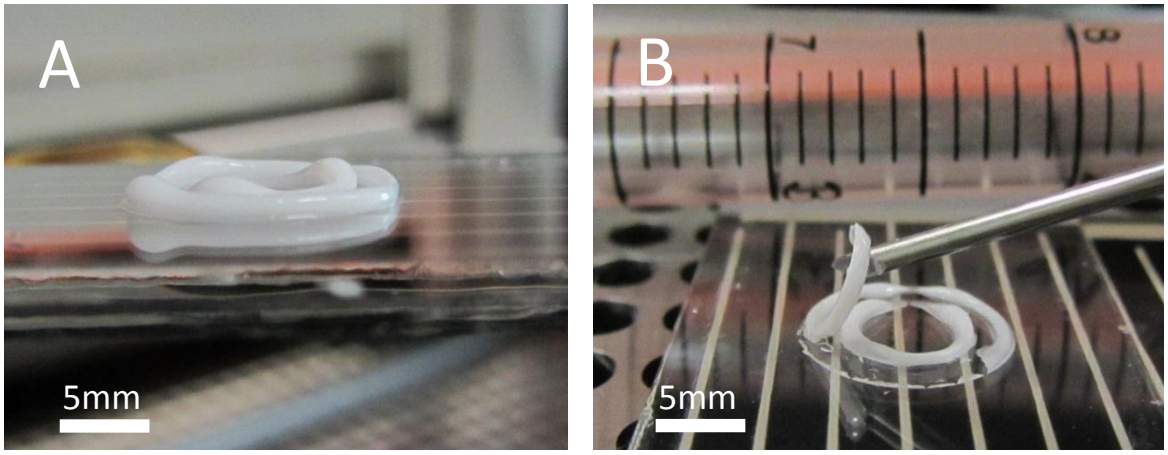

Figure 6.13. *3D printed circular structures were constructed from four individual layers. Two different ink blends were imaged A: HA-PNIPAM 15% + HAMA 2%, B: HA-PNIPAM 15% + HAMA 1%.*

Figure 6.14 illustrates the layered articular cartilage mimicking scaffold structure and the bioinks chosen for each layer (A, B, C). Like in the native articular cartilage the modulus increases when going deeper into the layers achieving its highest modulus on the surface of the subchondral bone. For this reason, the bottom layer was printed from HA-PNIPAM 15% + HAMA 2%, ink C, which was the toughest gel produced. To produce high modulus structures through the scaffold the rims of the second layers were printed also with the ink C and the inner structure was printed full with HA-PNIPAM 15% + HAMA 1%, ink B, to increase nutrient diffusion into the middle zone. The intermediate layer is seamlessly bound to the bottom layer due to continuous outer rim (ink C). This construct may be also easier to attach to the defect site in future applications due to one optimized binding method. The surface layer was printed with HA-PNIPAM 15% + CSMA 5%, ink A, which had high modulus but due to sulfate groups it also attracted more water into the structure. This swelling behavior could fix the scaffold to the defect walls by creating mechanical seal between the scaffold and native cartilage surface. Furthermore, the water content in the cartilage is decreasing when going deeper into the tissue similarly to this 3D cartilage scaffold. The swelling behavior was evaluated from bioink 1cm diameter scaffolds by diameter change after 24 hours in PBS. The ink A was swelling the most due to higher water affinity; however, neither

inks B or C showed any changes in diameter. Inks B and C were also binding substantial amount of water into their structures but due to long polymer chains of HA and the dense crosslinking network the printed dimensions were not swollen. This enables accurate size and shape printing and ensures conservation of the construct resolution.

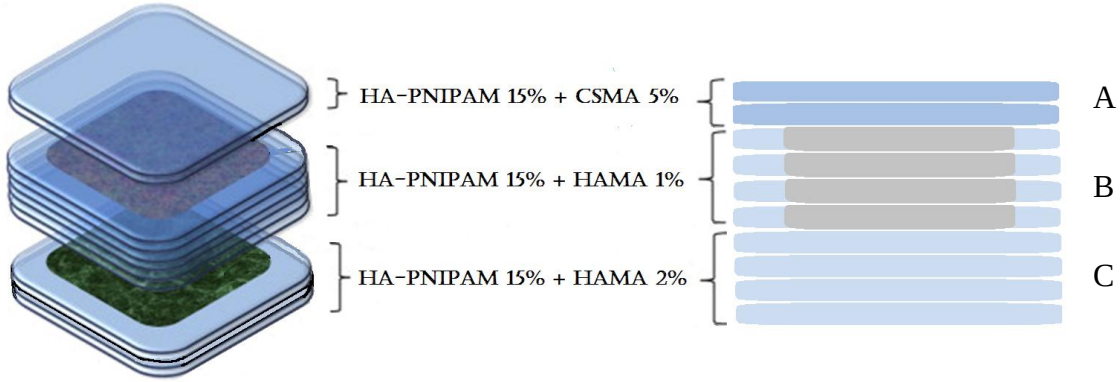

Figure 6.14. *Schematic picture of 3D layered scaffold that was designed to mimic the native cartilage structure.*

Figure 6.15 illustrates the printed structure of the previously discussed 3D articular cartilage layers mimicking scaffold. The structure was printed with bioinks incorporated with food dyes for illustration purposes. Figure 6.15A is obtained after the deep and intermediate layers were printed and UV-crosslinked. The construct is stable and the ink B is clearly filling the structure; however, the resolution is about 1mm in line thickness which is caused by the flow after printing. Figure 6.15B shows the printed and crosslinked scaffold with all three zones A, B and C. All three layers are clearly visible but the intermediate layers are higher from the middle compared to the sides creating bubble like surface. This behavior is a consequence from the intermediate layer being printed with too much material and the surface layer surface tensions before the gelling.

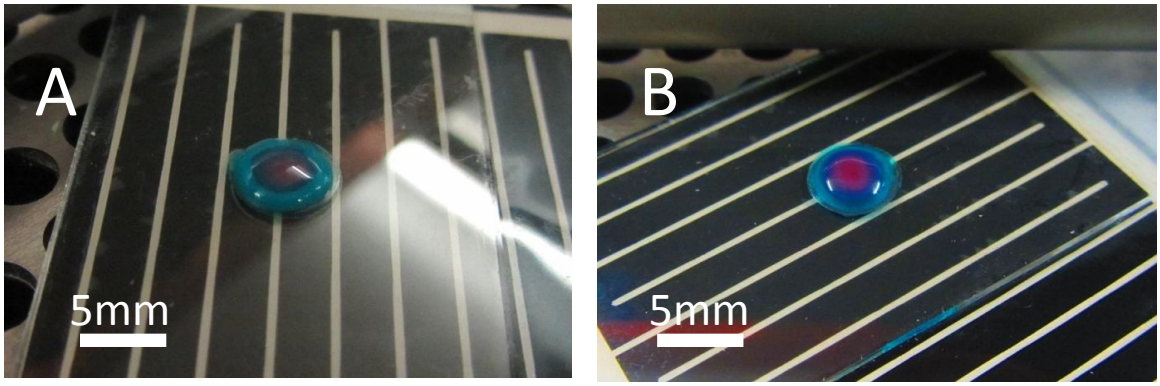

Figure 6.15. *3D printed native cartilage mimicking structure. Printing was made from three layered materials like illustrated in Figure 6.14. Image A is taken when both layers B and C were printed. Image B is taken from the final 3D construct.*

The 3D printed scaffold was produced as planned and it resembled the native cartilage structure. This structure should be further printed with the chondrocytes to investigate the resolution of the printing process with the cells included in the bioink and the viability after printing. Based on other studies the chondrocytes can be expected to survive the printing procedure (Xu et al,. 2013) although the resolution can be slightly affected by the lower modulus after temperature crosslinking with chondrocytes.

7. CONCLUSIONS

3D tissue printing is a new and revolutionary technique towards personalized medicine. With 3D bioprinting, a patient specific and uniquely designed tissue graft could be manufactured by means of MRI data. These designed tissue grafts would not only fit to the patient's defect but also mimic the native articular cartilage layered structure. These layers vary significantly throughout the structure in terms of modulus, cell concentration and water content (Blitterswijk et al. 2008).

The aim of this thesis was to investigate different material combinations to be used as bioinks for cartilage production. The mechanical properties of the crosslinked gels were analyzed and compared in different biopolymer concentrations. The results illustrated that the biopolymer concentration had a significant influence on the properties of the bioink in crosslinking and in the final product. Increased polymer concentration had generally a limiting effect on thermoresponsive crosslinking. This was assumed to result from the reduced free space inside the material, preventing the PNIPAM side chains from interacting and forming the crosslinking network. Although, in HA-PNIPAM + DEXMA materials this effect was not significant but also distinguished. In general the HA-PNIPAM + CSMA had the lowest thermoresponsive crosslinking due to the electrostatic charge of the sulfate molecule. All the mixtures that had the thermoresponsive behaviour were crosslinked at body temperature (37°C). Furthermore, the UV crosslinking was effective in all the other materials apart from HA-PNIPAM + DEXMA mixtures with a DEXMA content under 5%. Interestingly we could identify inversely proportional crosslinking behavior in the materials. Mixtures more sensitive to temperature increasing were crosslinking less in UV exposure despite the initiator concentration. This result illustrates how important the polymer chain movement is. If the movement is limited, the physical crosslinking in UV exposure cannot proceed.

Cell viability assays were showing good results in higher polymer concentrations compared to the lower. This result was hypothesized could the softness of the gel be the reason to lower viabilities. Chondrocytes are in thick ECM matrix in the native cartilage which could explain why the viability was higher in the thicker biopolymers. Based on these results as well as rheology analyses the promising gel mixtures were chosen and tested for 3D bioprinting. Furthermore, different constructs and printed composite structures were created and analyzed. For each bioink the bioprinter parameters had to be optimized. This is one of the drawbacks of this technology requiring specific parameters to be optimized for each individual inks used. After the trials we were able to produce 3D, three layered composite scaffold by using these bioinks.

The composite construct was stable and the bioink layers stayed separate. Individual tandem crosslinked bioinks held the resolution of the printing and had increased modulus after UV curing.

The future work with these bioinks should consider the development of the mechanical properties of the scaffold. The rheology data illustrates over three order of magnitude difference compared to native cartilage modulus. This significant difference could be overtaken by introducing fiber reinforcements or particles into the matrix. The composite construct reinforced with collagen fibers could stand greater compressive loading. Furthermore, the cell viability studies should be conducted for the printed constructs to verify the cell survival from the printing. Also the autofluorescence problem of HA-PNIPAM in live/dead staining should be assessed. Possible solution could be the use of the MTT assays or histological staining. The third path of investigation could study the improvement of the resolution of the printing and the fast gelation by increasing the temperature. Minor challenges such as drying, swelling and costs should be also assessed and investigated for future materials to be more easily accepted in applications.

REFERENCES

(Ashammakhi et al. 2007) N. Ashammakhi, R. Reis and E. Chiellini. 2007 Topics in Tissue Engineering, Vol 3, Chapter 1 p.37

(Becerra et al. 2010) Becerra Jose, Andrades A. Jose, Guerado Enrique, Zamora-Navas Placido, Lopez-Puertas Jose and Reddi Hari. 2010, Articular cartilage : structure and regeneration. Tissue Engineering, vol.16, pp. 617-627.

(Billiet et al. 2012) Billiet, T., M. Vandenhaute, J. Schelfhout, S. Van Vlierberghe and P. Dubruel. 2012, A review of trends and limitations in hydrogel-rapid prototyping for tissue engineering. Biomaterials 33, vol.26, pp. 6020-6041.

(Blitterswijk et al. 2008) Clement van Blitterswijk, Peter Thomsen, Anders Lindahl, Jeffrey Hubbell, David F. Williams, Ranieri Cancedda, Joost D. de Bruijn and Jerome Sohier 2008. Tissue Engineering. Academic Press p.760

(Burdick et al. 2005) Jason A. Burdick, Cindy Chung, Xinqiao Jia, Mark A. Randolph, Robert Langer. 2005, Controlled degradation and mechanical behavior of photopolymerized hyaluronic acid networks. Biomacromolecules 6, pp. 386-391.

(Burdick et al. 2011) Burdick, J. A. and G. D. Prestwich. 2011, Hyaluronic acid hydrogels for biomedical applications. Adv Materials 23, vol.12, pp. 41-56.

(Burdick and Murphy, 2012) Burdick, J. A. and W. L. Murphy. 2012, Moving from static to dynamic complexity in hydrogel design. Nat Commun, vol.3, pp. 1269.

(Ceresa, 2012) Brian P. Ceresa. 2012, Molecular Regulation of Endocytosis, InTech, p. 466.

(Chaterji et al. 2007) Chaterji, S., I. K. Kwon and K. Park. 2007, Smart Polymeric Gels: Redefining the Limits of Biomedical Devices. Prog Polym Sci 32(8-9), pp. 1083-1122.

(Chung and Park, 2009) Hyun Jung Chung, Tae Gwan Park. 2009, Self-assembled and nanostructured hydrogels for drug delivery and tissue engineering. Nano Today, vol.4, pp. 429-437.

(Chung, 2009) Chung Cindy. Development and characterization of photocrosslinkable hyaluronic acid hydrogels for cartilage regeneration (2009). Publicly accessible Penn Dissertations. Paper 24. Source: http://repository.upenn.edu/edissertations/24.

(D'Arrigo et al. 2012) Giorgia D'Arrigo, Chiara Di Meo, Erik Geissler, Tommasina Coviello, Franco Alhaique and Pietro Matricardi. 2012, Hyaluronic acid methacrylate derivates and calcium alginate interpenetrated hydrogel networks for biomedical applications: physic-chemical characterization and protein release. Colloid Polym. Sci., vol.290, pp. 1575-1582.

(D'Este et al. 2012) D'Este, M., M. Alini and D. Eglin. 2012, Single step synthesis and characterization of thermoresponsive hyaluronan hydrogels. Carbohydrate Polymers 90, vol.3, pp. 1378-1385.

(Durango) Durango Orthopaedics, Durango Colorado, web copyright 2009 Prizm. Available from: http://www.durangoorthopedics.com/assets/images/knee_cartilage.jpg

(Fairbanks et al. 2009) Benjamin D. Fairbanks, Michael P. Schwartz, Christopher N. Bowman, Kristi S. Anseth. 2009, Photoinitiated polymerization of PEG-diacrylate with lithium phenyl-2,4,6-trimethylbenzoylphosphinate: polymerization rate and cytocompatibility. Biomaterials, pp. 6702–6707.

(Fedorovich et al. 2007) Fedorovich, N. E., J. Alblas, J. R. de Wijn, W. E. Hennink, A. J. Verbout and W. J. A. Dhert. 2007, Hydrogels as extracellular matrices for skeletal tissue engineering: state-of-the-art and novel application in organ printing. Tissue Engineering 13 vol.8, pp. 1905-1925.

(Ferris et al. 2013) Gameron Ferris, Kerry Gilmore, Stephen Beirne, Donald McCallum, Gordon G. Wallace and Marc in het Panhuis. 2013, Bio-ink on demand printing of living cells. Biomaterial Sci. 2 vol. 1, pp. 224-230.

(Foldager et al. 2011) Casper Foldager, Anna Nielsen, Samir Munir, Michael Ulrich-Vinther, Kjeld Soballe, Cody Bünger and Martin Lind. 2011, Combined 3D and hypoxic culture improves cartilage-specific gene expression in human chondrocytes. Acta Orthopaedica 82 vol. 2, pp. 234-240.

(Fosang et al. 1992) Fosang, A. J., P. J. Neame, K. Last, T. E. Hardingham, G. Murphy and J. A. Hamilton. 1992, The interglobular domain of cartilage aggrecan is cleaved by PUMP, gelatinases, and cathepsin B. J Biol Chem 267, vol.27, pp. 19470-19474.

(Fulcher et al. 2009) Fulcher, G. R., D. W. L. Hukins and D. E. T. Shepherd. 2009, Viscoelastic properties of bovine articular cartilage attached to subchondral bone at high frequencies. Bmc Musculoskeletal Disorders 10.

(Gauvin et al. 2012) Robert Gauvin, Ying-Chieh Chen, Jin Woo Lee, Pranav Soman, Pinar Zorlutuna, Jason W. Nichol, Hojae Bae, Shaochen Chen and Ali Khademhosseini.

2012, Microfabrication of complex porous tissue engineering scaffolds using 3D projection stereolithoraphy. Biomaterials 15, vol. 33, pp. 3824-3834.

(Gigante et al. 2001) Gigante A., Bevilacqua C., Zara C., Travasi M., and Chillemi C. 2001, Autologous chondrocyte implantation: cells phenotype and proliferation analysis. Knee Surg Sports Traumatol Arthrosc 9, p.254.

(Goessler et al. 2006) U.R. Goessler, K. Bieback, P. Bugert, T. Heller, H. Sadick, K. Hörmann and F. Riedel. 2006, In vitro analysis of integrin expression during chondrogenic differentiation of mesenchymal stem cells and chondrocytes upon dedifferentiation in cell culture. International journal of molecular medicine, vol. 17,no. 2, pp 301-307.

(Hollister, 2005) Scott J. Hollister. 2005, Porous scaffold design for tissue engineering. Nature materials, vol. 4, pp.518-524.

(Landínez-Parra, 2012) Nancy S. Landínez-Parra, Diego A. Garzón-Alvarado and Juan Carlos Vanegas-Acosta (2012). Mechanical Behavior of Articular Cartilage, Injury and Skeletal Biomechanics, Dr. Tarun Goswami (Ed.), ISBN: 978-953-51-0690-6, InTech, DOI: 10.5772/48323. Available from: http://www.intechopen.com/books/injury-and-skeletal-biomechanics/-mechanical-behavior-of-articular-cartilage

(Leach et al. 2002) Jennie Baier Leach, Kathryn A. Bivens, Charles W. Patrick Jr. and Christine E. Schmidt. 2002, Photocrosslinked hyaluronic acid hydrogels: Natural, Biodegradable Tissue Engineering Scaffold. Biotechnology and bioengineering, vol.82, no.5, pp. 578-589.

(Lee et al. 2007) Seung-Young Lee , Giyoong Tae and Young Ha Kim. 2007, Thermal gellation and photo-polymerization of di-acrylated Pluronic F 127. Journal of Biomaterials Science, Polymer Edition, vol.18, no.10, pp. 1335-1353.

(Li et al. 2003) Qiang Li, Christopher G. Williams, Danny D. N. Sun, Jun Wang, Kam Leong and Jennifer H. 2003, Elisseeff Photocrosslinkable polysaccharides based on chondroitin sulfate. J Biomed Mater Res 68A, pp. 28-33.

(Li et al. 2011) Li, C., M. M. Alam, S. Bolisetty, J. Adamcik and R. Mezzenga. 2011, New biocompatible thermo-reversible hydrogels from PNiPAM-decorated amyloid fibrils. Chem Commun 47, vol.10, pp. 2913-2915.

(Malonne et al. 2005) Malonne, H., F. Eeckman, D. Fontaine, A. Otto, L. D. Vos, A. Moes, J. Fontaine and K. Amighi. 2005, Preparation of poly(N-isopropylacrylamide) copolymers and preliminary assessment of their acute and subacute toxicity in mice. Eur J Pharm Biopharm 61, vol.3, pp. 188-194.

(Mastbergen et al. 2002) S. C. Mastbergen, F. P. J. G. Lafeber, and J. W. J. Bijlsma. 2002, Selective COX-2 inhibition prevents proinflammatory cytokine-induced cartilage damage. Rheumatology, vol.41, no.7, pp. 801–808.

(MeNickle et al. 2008) MeNickle, A. G., M. T. Provencher and B. J. Cole. 2008, Overview of Existing Cartilage Repair Technology. Sports Medicine and Arthroscopy Review 16, vol.4, pp. 196-201.

(Mortisen et al. 2010) Mortisen, D., M. Peroglio, M. Alini and D. Eglin. 2010, Tailoring thermoreversible hyaluronan hydrogels by "click" chemistry and RAFT polymerization for cell and drug therapy. Biomacromolecules 11, vol.5 pp. 1261-1272.

(Müller et al. 2008) R. D. Müller, T. John, B. Kohl, A. Feldner, H. Zreiqat, W. Ertel, D. Laface, B. Hutchins, A. Oberholzer, and G. Schulze-Tanzil. 2008, Cartilage-Specific Matrix and Integrin Expression in Three-Dimensional Articular Chondrocyte Cultures Overexpressing Human Interleukin-10. Clinical Medicine: Arthritis and Musculoskeletal Disorders, pp. 21–32.

(Murphy et al. 2013) Sean V. Murphy, Aleksander Skardal and Anthony Atala. 2013, Evaluation of hydrogels for bio-printing applications. J Biomed Mater Res Part A, vol.101A, pp. 272-284.

(Peach et al. 2005) Peach CA., Carr AJ. and Loughlin J. 2005, Recent advances in the genetic investigation of osteoarthritis. Trends Mol Med, vol.4, pp. 186-191.

(Peltola et al. 2008) Peltola, S. M., F. P. Melchels, D. W. Grijpma and M. Kellomaki. 2008, A review of rapid prototyping techniques for tissue engineering purposes. Ann Med 40, vol.4, pp. 268-280.

(Peroglio et al. 2012) Peroglio, M., S. Grad, D. Mortisen, C. M. Sprecher, S. Illien-Junger, M. Alini and D. Eglin. 2012, Injectable thermoreversible hyaluronan-based hydrogels for nucleus pulposus cell encapsulation. Eur Spine J 21 Suppl 6, pp. 839-849.

(Schulze-Tanzil, 2009) G. Schulze-Tanzil. 2009, Activation and dedifferentiation of chondrocytes: implications in cartilage injury and repair. Annals of anatomy = Anatomischer Anzeiger : official organ of the Anatomische Gesellschaft, vol.191, no.4, pp. 325–338.

(Smeds et al. 2001) Kimberly A. Smeds, Mark W. Grinstaff. 2001, Photocrosslinkable polysaccharides for in situ hydrogel formation. Journal of Biomedical Materials Research, 54, pp. 115–121.

(Stern et al. 2006) Robert Stern, Akira A. Asari and Kazuki N. Sugahara. 2006, Hyaluronan fragments: An information-rich system. European journal of cell biology. 85, pp. 699-715.

(Temenoff and Mikos, 2000) Temenoff, J. S. and A. G. Mikos. 2000, Review: tissue engineering for regeneration of articular cartilage. Biomaterials 21, vol.5, pp. 431-440.

(Turunen et al. 2011) Sanna Turunen, Anne-Marie Haaparanta, Riikka äänismaa and Minna Kellomäki. 2011, Chemical and topographical patterning of hydrogels for neural cell guidance in vitro. Journal of tissue Eng. Regen. Med. 4, vol. 7, pp. 253-270.

(Vincent and Watt, 2010) Vincent TL. and Watt FE. 2010, Osteoarthritis. Medicine 38, vol 3., pp. 151-156.

(Warrell et al. 2010) David A. Warrell, Timothy M. Cox and John D. 2010, Firth. Oxford textbook of medicine. 5th edn. Oxford. Oxford university press. p. 6016.

(Xu et al,. 2013) Xu T., Binder K. W., Albanna N. Z., Dice D., Zhao W., Yoo J. J. and Atala A. 2013, Hybrid printing of mechanically and biologically improved constructs for cartilage tissue engineering applications. Biofabrication, vol.5, Issue 1, pp. 1-10.

(Yamada et al. 1990) N. Yamada, T. Okano, H. Sakai, F. Karikusa, T. Sawasaki and Y. Sakurai. 1990, Thermo-responsive polymeric surfaces; control of attachment and detachment of cultured cells, Makromol. Chem. Rapid. Commun. 11, pp. 571-576.

(Zhang et al. 2008) Linna Zhang, Shengmao Zhang, Benfang He, Zhishen Wu and Zhijun Zhang. 2008, TiO_2 Nanoparticles functionalized by a temperature-sensitive poly(N-isopropylacrylamide) (PNIPAM): Synthesis and characterization. Z. Naturforschung, 63b, pp. 973-976.

APPENDIX 1: HA-PNIPAM FULL ^{1}H-NMR SPECTRA

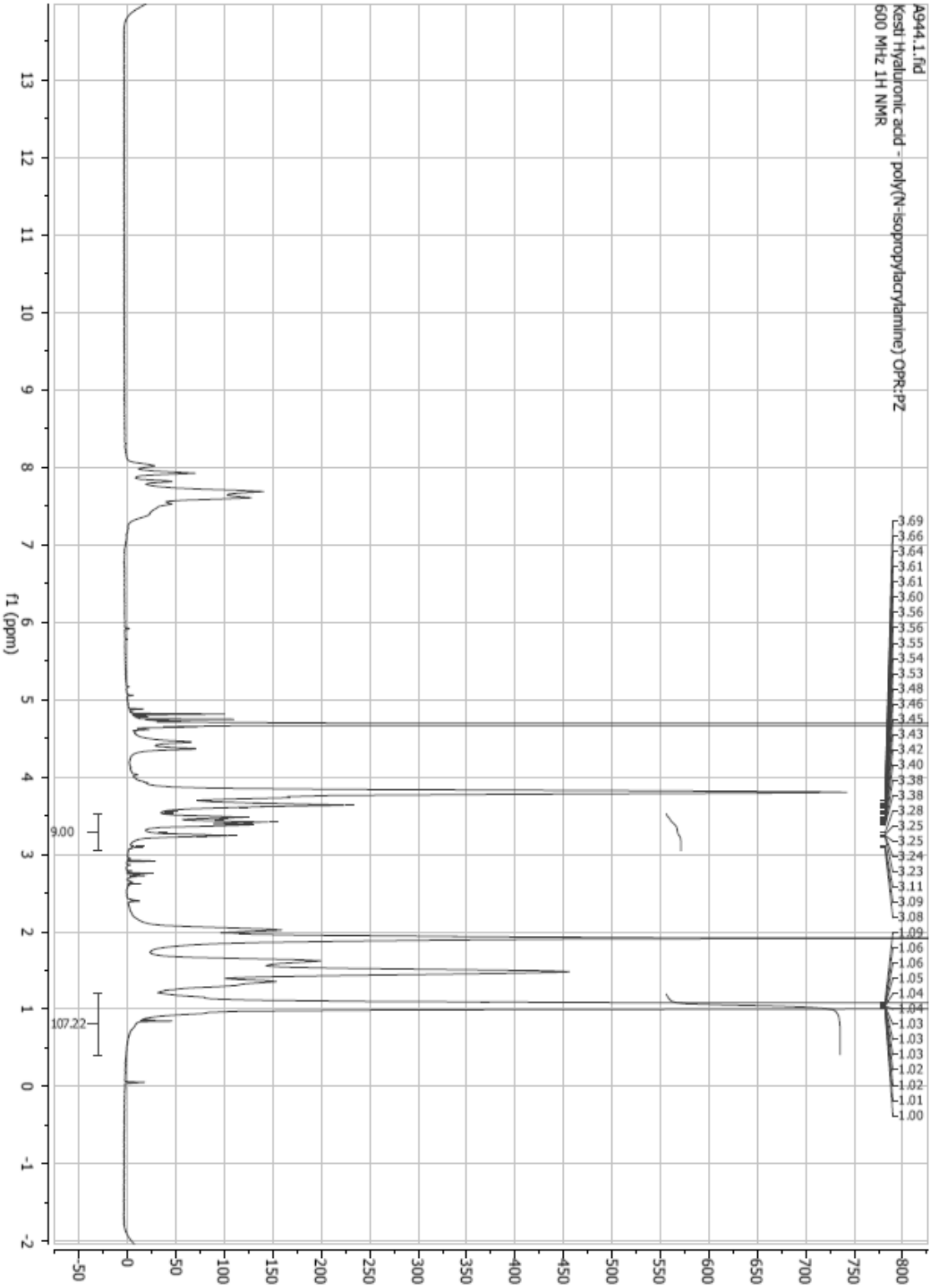

APPENDIX 2: HAMA FULL ^{1}H-NMR SPECTRA